

X-625-73-355

PREPRINT

NASA TM X- 70586

**A STUDY OF ELECTRON DENSITY
PROFILES IN RELATION
TO IONIZATION SOURCES
AND GROUND-BASED RADIO WAVE
ABSORPTION MEASUREMENTS,
PART I**

S. GNANALINGAM

J. A. KANE

(NASA-TM-X-70586) A STUDY OF ELECTRON
DENSITY PROFILES IN RELATION TO
IONIZATION SOURCES AND GROUND-BASED RADIO
WAVE ABSORPTION MEASUREMENTS, PART 1
(NASA) 76 p HC \$7.00

N74-17119

CSCI 20N

G3/13

Unclas
30705

NOVEMBER 1973



GODDARD SPACE FLIGHT CENTER
GREENBELT, MARYLAND

A STUDY OF ELECTRON DENSITY PROFILES IN RELATION TO
IONIZATION SOURCES AND GROUND-BASED RADIO WAVE ABSORPTION
MEASUREMENTS, PART I.

by

C. Gnanalingam*

and

J. A. Kane

Laboratory for Planetary Atmospheres
NASA/Goddard Space Flight Center
Greenbelt, Maryland

ABSTRACT

In this work an extensive set of ground-based measurements of the diurnal variation of medium frequency radio wave absorption and virtual height is analysed in terms of our current understanding of the D- and lower E-region ion production and loss process. When this is done a gross discrepancy arises, the source of which is not known.

*Present address: Ceylon Institute of Scientific
and Industrial Research
P. O. Box 787
Colombo, Sri Lanka (Ceylon)

CONTENT(continued)

<u>Appendix</u>		<u>Page</u>
A-4	Number of Molecules Along Line of Sight	43
A-5	$Q(z, \chi)$ Components and r.m.s. Error	47
A-6	Reference Electron Density Profile	51
A-7	Calculated $N_e(z, \chi)$	59
A-8	Required $N_e(z, \chi)$	65
Acknowledgement	67
References	68

A STUDY OF ELECTRON DENSITY PROFILES IN RELATION TO IONIZATION SOURCES AND GROUND-BASED RADIO WAVE ABSORPTION MEASUREMENTS, PART I

1. INTRODUCTION

In recent years computer modelling of photo-chemical processes has become one of the primary tools for advancing our understanding of the lower ionosphere. Since the early work of Keneshea (1967) computer models have been continually updated and expanded as more and more reaction rate coefficients and cross sections have become known from laboratory measurements. Unfortunately in many cases it is not possible to adequately test the predictions of a particular time-dependent chemical model by comparison with results from rocket-borne in situ measurements. This is because, from a practical standpoint, rocket measurements cannot be made frequently enough to accurately trace the time dependence of the experimental quantity. However, as will be brought out in this report, our knowledge of at least one of the more important quantities, namely the electron density profile and its time dependence becomes much more precise when the results of in situ measurements can be combined with quantitative ground-based measurements of radio wave absorption.

Extensive multi-frequency absorption data have been obtained for the equatorial region over a long period of years by Gnanalingam (1972). Near the equator the anomalous day-to-day variability so characteristic of the mid-latitude winter mesosphere seems to be either absent or at least greatly reduced. It is well established that mesospheric pressures, densities and temperature undergo significant variation, both day-to-day as well as seasonal. The magnitude of both these variations however are smallest at lowest latitudes. This meteorological stability together with the presumed absence of energetic particle precipitation makes the equator the preferred location from which to study the build-up and decay of the lower ionosphere when it is under a simple solar zenith angle control.

With the large body of absorption data available for the equator as our control, we propose two objectives: (1) to deduce from a consideration of ion-pair production and loss processes the diurnal variation of the D- and lower E-region electron density profile for the conditions of an undisturbed sun at solar cycle maximum; and (2) to deduce the noontime electron density profile for the conditions of a moderately disturbed sun. Objective (2) will be the subject of a separate report which we hope to publish later. In the present work we take up

objective (1) which we pursue as follows: We first construct the best possible noontime reference electron density profile by combining the results of a rocket-borne experiment with the results of a series of ground-based multi-frequency absorption measurements. Next, from our current knowledge of ionization sources, we calculate the noontime profile of the ion-production function. These two steps immediately define the noontime profile of α_{eff} , the effective electron recombination coefficient. We now assume that this profile of α_{eff} is time independent. From the calculated solar zenith angle dependence of the ion-production function, we can then predict the decay of the electron density profile as the solar zenith angle moves toward sunset. Finally our predictions are tested against highly accurate measurements of the diurnal variation of radio-wave absorption. The work is organized as follows:-

In section 2 we compile an atmospheric model which is representative of the equatorial region during equinoctial months. The model up to 95 km is taken directly from the tables given by Groves (1971) and extended to 160 km by means of the data given by Jacchia (1971). For the important minor constituent nitric oxide, we use the profile of Meira (1970).

In section 3 we describe our electron collision frequency profile which is derived from the atmospheric model of section 2. Included in this collision frequency profile are first order correction terms for the effects of electron collisions with ions and with oxygen atoms.

In section 4 we consider the solar radiations that govern the ion production function in the lower ionosphere. It is found that our knowledge concerning the variation of the X.U.V. flux with solar activity is rather poor. This situation is unfortunate since it makes it difficult to extrapolate flux measurements to different levels of solar activity. Nevertheless we proceed in section 5 to calculate our ion production function versus altitude and solar zenith angle using what we think are the most appropriate values of solar X.U.V. flux for the conditions of an undisturbed sun at solar cycle maximum.

In section 6 results from a noontime rocket measurement at Thumba, India are combined with the results of multi-frequency absorption and virtual height measurements made at Colombo, Ceylon on 72 selected days. This combination of in situ and ground-based measurements is used to construct a reference electron density profile for a solar zenith angle $\chi = 10^\circ$ for the conditions of an undisturbed sun at solar cycle maximum. By combining this reference electron density profile $N_e(\text{ref.})$ with the ion production function $Q(10^\circ)$ calculated for $\chi = 10^\circ$, we can define an effective recombination coefficient $\alpha_{eff} = Q(10^\circ)/N_e^2(\text{ref.})$. Our altitude profile of α_{eff} and its implications are discussed in section 7.

In section 8, starting with the reference electron density profile as an initial condition, the solar zenith angle dependence of the electron density N_e is calculated by numerically solving the familiar equation:

$$dN_e/dt = Q(\chi) - \alpha_{eff} N_e^2$$

where $Q(\chi)$ is the ion production function computed in section 5.

From the electron density profiles of section 8 together with the collision frequency model of section 3 we can calculate the solar zenith angle dependence of radio wave absorption and virtual reflection height. This is done in section 9 where we find that when the calculated values are compared against the measured diurnal variations, a gross discrepancy is revealed. Until this discrepancy is resolved, which we have not been able to do, our understanding of the basic processes of the lower ionosphere must be considered unsatisfactory.

Finally, in section 10, for the sake of completeness, we construct an ad hoc set of $N_e(z, \chi)$ profiles which yield agreement with the measured diurnal variation of absorption and virtual height. It is believed that this set of profiles can provide a fairly stringent test for any theory of the lower ionosphere.

2. ATMOSPHERIC MODEL

Although we shall calculate the ion production function only to 110 km, we need an atmospheric model to at least 160 km to determine the attenuation of solar flux. The time independent atmospheric model which is used throughout the present work is based on the lower altitude data of Groves (1971) for 10° latitude at equinox, and extrapolated to 160 km by means of the Jacchia (1971) model for an exospheric temperature of 1100 degrees Kelvin. This value of exospheric temperature was chosen so as to be consistent with a 10.7 cm solar flux level of 135 units, i.e. the solar condition under which our radio wave absorption measurements were obtained. Details of the model together with tabulated values are given in appendix A-1.

3. COLLISION FREQUENCY MODEL

The collision frequency model used in the present work is based on the recent review of Phelps (1972). For the ionospheric temperatures with which we are concerned, monoenergetic electron collision frequencies for the major constituents N_2 and O_2 can be combined conveniently into the expression

$$\nu_p = (6.5 \pm 0.7) \times 10^5 p_{mks}$$

where p_{mks} is the gas pressure in newton/m². Above 90 km it is advisable to include first order correction terms for the effects of electron collisions with ions and electron collisions with atomic oxygen. The electron-ion collision frequency (Phelps, 1972) is given by

$$\nu_{ie} = 3.6 N_e T_e^{-1.5} \times \ln(2 \times 10^4 T_e^{1.5} / N_e^{0.5})$$

where N_e and T_e are the electron density (cm⁻³) and temperature (°K) respectively. To obtain the electron-atomic oxygen collision frequency ν_{eo} , we use a theoretical expression given by Banks (1966) for the average momentum transfer cross section σ_{eo} , i.e.,

$$\sigma_{eo} = (3.4 \pm 1.0) \times 10^{-16} \text{ cm}^2$$

For ν_{eo} we then have

$$\begin{aligned} \nu_{eo} &= [O] \sigma_{eo} \bar{v}_e \\ &= [O] \times \{1.88 \times 10^{-10} T_e^{0.5}\} (1 \pm .3) \end{aligned}$$

where $[O]$ is the density (cm⁻³) of atomic oxygen.

The total collision frequency $\nu = \nu_p + \nu_{ei} + \nu_{eo}$ and its components are listed in appendix A-2.

For the purpose of computing radio wave absorption, we use in the conductivity integrals the value of collision frequency given by $\nu = \nu_p + \nu_{ei} + \nu_{eo}$. Strictly speaking this is incorrect since it ignores the different energy dependence of the three components of ν . However, in our case the radio waves are all reflected from altitudes below 105 km, where ν_{ei} and ν_{eo} are small correction terms. Hence the neglect of their different energy dependence should not lead to any significant error in our calculated values of absorption.

4. SOLAR RADIATIONS

A considerable volume of literature has been written concerning the solar radiations that are effective ionization sources for the D- and lower E-regions of

the ionosphere; see for example the reviews of Ohshio et al (1966), Ivanov-Kholodnyi and Nikol'skii (1969), Swider (1969), Aikin (1972). For the altitude region of concern in the present work, i.e. from 60-110 km, the major ionizing radiations are

- (a) the hydrogen Lyman- α line (1215.7A).
- (b) the hydrogen Lyman- β line (1025.7A) together with the nearby continuum in the 1025-990A interval,
- (c) the carbon III line at 977A and
- (d) soft X-rays in the wavelength interval 100-1A.

The intensity of a particular radiation can be expected to vary considerably with solar activity. This is particularly true for wavelengths less than 10A. In appendix A-3 we give a brief survey of the present state of knowledge concerning these solar fluxes. Based on that survey the flux values used in the present work are listed in table I for the conditions of an undisturbed sun at solar cycle maximum.

In Fig. 1 the energy flux values for the range 100-1A are normalized to unit energy interval of 1eV ($\phi F / \delta U$ in table I) and plotted versus energy. For the energy range corresponding to 100-30A (i.e. $124 \leq U \leq 413$ eV) our tabulated fluxes are based primarily on the most recent values given by Manson (1972) which have a claimed accuracy of $\pm 25\%$. Below 10A (i.e. $U > 1240$ eV) our tabulated flux values are obtained by fitting satellite measurements of the 1-8A energy flux to a bremsstrahlung type spectrum for a coronal temperature of 3.5×10^6 degrees K. (This is discussed in appendix A-3.) For the range 30-10A ($413 \leq U \leq 1240$ eV) our tabulated fluxes are given by the arbitrary straight line of Fig. 1 which connects Manson's values above 30A with the bremsstrahlung-type spectrum values below 10A. Fortunately our choice of flux values in the 30-10A range does not strongly affect our calculated value of the ion production function, as we shall see in the following section.

TABLE I
Estimated Solar Flux*

Wavelength (Angstroms)	Energy U (eV)	\bar{U} (eV)	Energy Flux δF (ergs/cm ² sec)	Photon Flux (ph/cm ² sec)	$\delta F/\delta U$ (eV/cm ² sec eV)
1215.7 (Ly- α)	10.20		5.4×10^0	3.3×10^{11}	
1025.7 (Ly- β)	12.09		7.0×10^{-2}	3.6×10^9	
1025 - 990	12.1 - 42.5	12.32	8.3×10^{-2}	4.2×10^9	
977 CIII	12.69		9.0×10^{-2}	4.4×10^9	
103 - 83	120 - 149	135	4.9×10^{-2}	2.3×10^8	1.06×10^9
83 - 62	149 - 200	175	5.7×10^{-2}	2.0×10^8	7.0×10^8
62 - 41	200 - 302	251	4.9×10^{-2}	1.2×10^8	3.0×10^8
41 - 31	302 - 400	351	1.5×10^{-2}	2.6×10^7	9.4×10^7
31 - 23	400 - 539	470	9.1×10^{-3}	1.2×10^7	4.1×10^7
23 - 20	539 - 620	580	3.5×10^{-3}	3.8×10^6	2.7×10^7
20 - 15	620 - 827	724	5.3×10^{-3}	4.6×10^6	1.6×10^7
15 - 10.5	827 - 1181	1004	3.2×10^{-3}	2.0×10^6	5.6×10^6
10.5 - 9.5	1181 - 1305	1243	4.6×10^{-4}	2.3×10^5	
9.5 - 8.5	1305 - 1459	1382	3.5×10^{-4}	1.6×10^5	
8.5 - 7.5	1459 - 1653	1556	2.6×10^{-4}	1.0×10^5	
7.5 - 6.5	1653 - 1908	1781	1.6×10^{-4}	5.7×10^4	
6.5 - 5.5	1908 - 2255	2082	8.3×10^{-5}	2.5×10^4	
5.5 - 4.5	2255 - 2756	2506	3.0×10^{-5}	7.6×10^3	
4.5 - 3.5	2756 - 3543	3150	6.1×10^{-6}	1.2×10^3	
3.5 - 2.5	3543 - 4960	4252	3.6×10^{-7}	5.3×10^1	
2.5 - 1.5	4960 - 8267	6614	8.8×10^{-10}	8.3×10^{-2}	
1.5 - 0.5	8267 - 24800	16534	5.0×10^{-18}	1.9×10^{-10}	

* Solar cycle maximum, non-flare conditions: 1-8A energy flux = 4×10^{-4} erg/cm² sec
sunspot number ≈ 100
10.7 cm flux $\approx 135 \times 10^{-22}$ W/m² Hz

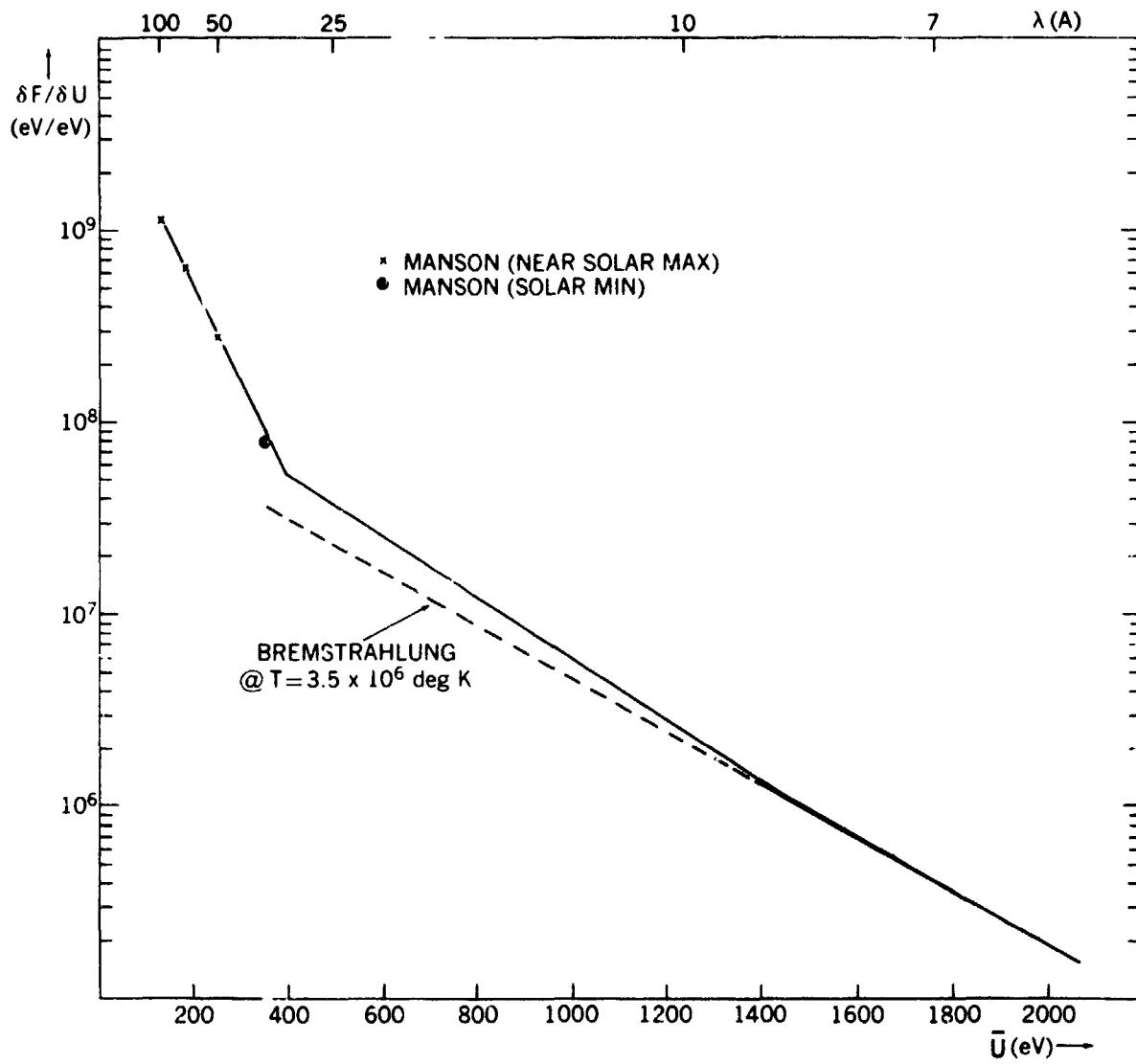


Figure 1. Solar energy flux per unit energy versus photon energy.

5. ION PRODUCTION FUNCTION

The total ion-production function $Q(z, \chi)$ at an altitude z and solar zenith angle χ is the sum of many separate production functions, each for a particular wavelength or wavelength band, i.e.

$$Q(z, \chi) = \sum_{\lambda} q_{\lambda}(z, \chi)$$
$$q_{\lambda}(z, \chi) = F_{\lambda}(z, \chi) \sum_j \gamma_{\lambda j} \sigma_{\lambda j} N_j(z)$$

where we define

$F_{\lambda}(z, \chi)$: value of the attenuated solar flux at wavelength λ

$N_j(z)$: number density of the j constituent of the atmosphere.

$\sigma_{\lambda j}$: cross section at wavelength λ for photon absorption by a molecule of species j .

$\gamma_{\lambda j}$: photoionization yield, i.e. the number of electron-ion pairs formed when one photon of wavelength λ is absorbed by a molecule of species j .

5.1 Absorption Cross Sections and Ionization Yields

The subject of photon absorption cross sections and ionization yields in the wavelength range 100-1A has been elucidated in the previously mentioned review by Swider (1969)*. Based on the formulas quoted in that review together with additional tabulations given by Ohshio et al (1966), the values used in the present work are listed in Table II for the atmospheric constituents O, O₂, N₂ and NO.

* Recent work by Henke and Elgin (1970) has substantiated the formulas quoted by Swider (1969) which date back to the year 1933.

TABLE II
Absorption Cross Sections and Ionization Yields

λ (A)	$\sigma(O)$ (cm ²)	$\sigma(O_2)$ (cm ²)	$\sigma(N_2)$ (cm ²)	$\gamma(O)$	$\gamma(O_2)$	$\gamma(N_2)$
1	8.43E ⁻²³	1.76E ⁻²²	1.03E ⁻²²	340	340	384
2	6.40E ⁻²²	1.31E ⁻²¹	7.47E ⁻²²	158	158	179
3	2.20E ⁻²¹	4.29E ⁻²¹	2.46E ⁻²¹	99.2	99.2	112
4	5.02E ⁻²¹	9.93E ⁻²¹	5.73E ⁻²¹	69.7	69.7	78.9
5	1.00E ⁻²⁰	1.90E ⁻²⁰	1.10E ⁻²⁰	52.5	52.5	59.4
6	1.67E ⁻²⁰	3.20E ⁻²⁰	1.87E ⁻²⁰	41.1	41.1	46.6
7	2.65E ⁻²⁰	4.94E ⁻²⁰	2.76E ⁻²⁰	33.3	33.3	37.7
8	3.80E ⁻²⁰	7.22E ⁻²⁰	4.27E ⁻²⁰	27.4	27.4	31.0
9	5.40E ⁻²⁰	1.01E ⁻¹⁹	5.70E ⁻²⁰	23.0	23.0	26.0
10	6.90E ⁻²⁰	1.34E ⁻¹⁹	8.05E ⁻²⁰	19.2	19.2	21.8
10-15	1.18E ⁻¹⁹	2.70E ⁻¹⁹	1.50E ⁻¹⁹	16.7	16.7	18.9
15-20	2.68E ⁻¹⁹	7.00E ⁻¹⁹	3.60E ⁻¹⁹	13.5	13.5	15.2
20-23	3.50E ⁻¹⁹	7.00E ⁻¹⁹	3.60E ⁻¹⁹	11.8	11.8	13.3
23-31	4.50E ⁻²⁰	9.00E ⁻²⁰	1.00E ⁻¹⁸	10.1	10.1	11.4
31-103	see footnote*					
977	0	2.98E ⁻¹⁸	8.20E ⁻²⁰	0	0.62	0
990-1025	0	1.75E ⁻¹⁸	7.40E ⁻²⁰	0	0.413	0
1025.7	0	1.52E ⁻¹⁸	1.00E ⁻²¹	0	0.58	0
1215.7	0	9.00E ⁻²¹	6.00E ⁻²³	0	0	0
1215.7		$\sigma(NO) = 2.40E^{-18}$			$\gamma(NO) = 0.81$	

* For the important wavelength interval 103-31A we take:

$$\sigma(O_2) = 2\sigma(O) = 2.27 \times 10^{-23} \lambda^{2.5} \text{ cm}^2$$

$$\sigma(N_2) = 1.33 \times 10^{-23} \lambda^{2.5} \text{ cm}^2$$

$$\gamma(O_2) = \gamma(O) = 1.02 + 273 \lambda^{-1}$$

$$\gamma(N_2) = 1.15 + 306 \lambda^{-1}$$

5.2 Number of Molecules Along Line of Sight

In order to calculate the ion production function at an altitude z for a given solar zenith angle χ , we need to know how the photon flux at a particular wavelength λ is attenuated along its path from the sun to the altitude z . This we can write as

$$F_{\lambda}(z, \chi) = F_{\lambda}^{(\infty)} \exp \left\{ - \sum_j \sigma_{\lambda j} \int_z^{L(\chi) \rightarrow \infty} N_j(L) dL \right\}$$

where $F_{\lambda}^{(\infty)}$ is the photon flux at the wavelength λ incident on the top of the atmosphere (table I), and dL is an element of the line of sight from altitude z to the sun. Assuming that our atmospheric model of section 2 is spherically symmetric, the calculation of $S(z, \chi)$, the number of molecules along the line of sight to the sun, defined by

$$S(z, \chi) = \int_z^{L(\chi) \rightarrow \infty} N_j(L) dL$$

is a straight-forward exercise in plane geometry, the details of which are given in appendix A-4. In that same appendix we also tabulate for several solar zenith angles the $S(z, \chi)$ values for the three atmospheric constituents N_2 , O_2 and O .

We have now covered all the material necessary to enable us to compute the major components of the ion production function for the lower ionosphere. Before we discuss the results of such calculations however, we shall consider briefly some additional sources of ionization that are included in our calculation of the total Q -function.

5.3 Additional Ionization Sources

In addition to the q_λ components computed from the flux values of table I and the cross section data of table II our total Q-function includes contributions from:

5.3.1 Scattered Radiation

As is well known scattered Lyman- α and scattered Lyman- β are major ionization sources for the lower ionosphere during nighttime. What may not be obvious is that these sources are not completely negligible during daytime, especially at high solar zenith angles near twilight. To calculate the q due to scattered Lyman alpha and scattered Lyman beta we assume as a first approximation that these sources are isotropically distributed over the upper hemisphere of the sky. The calculation of the $q_{\text{scat}}(z)$ for scattered radiation is then only slightly more complicated than the calculation of $q(\chi, z)$ for direct radiation, in that $q_{\text{scat}}(z)$ involves an additional integration over a local zenith angle θ , i.e.

$$q_{\text{scat}}(z) = \int_0^{\pi/2} q(\theta, z) \sin \theta d\theta$$

For the intensity of daytime scattered Lyman alpha we use the twilight value of 15 kilorayleigh (Meier and Mange, 1970). The scattered flux incident upon the top of the atmosphere is then approximately 2% of the value for direct solar Lyman alpha flux. Assuming this same ratio of scattered to direct flux, we take the intensity of the daytime scattered Lyman beta to be 150 rayleigh.

5.3.2 Metastable $O_2^*(^1\Delta_g)$

To account for the ionization of the metastable oxygen state $O_2^*(^1\Delta_g)$ by solar radiation near 1108A, we have used the formula given by Paulsen et al (1971).

$$q^*(z, \chi) = ND^*(z) \{0.549 \times 10^{-9} \exp(-2.406 \times 10^{-20} S_{O_2}(z, \chi)) \\ + 2.614 \times 10^{-9} \exp(-8.508 \times 10^{-20} S_{O_2}(z, \chi))\}$$

where $ND^*(z)$ is the $O_2^*(^1\Delta_g)$ number density and S_{O_2} is the number of O_2 molecules along the line of sight. This formula takes account of the attenuation of the 1108A flux by the minor constituent carbon dioxide. The authors of this formula estimate that there is an uncertainty of a factor of two on q^* due to uncertainties both in the 1108A flux and in the cross sections that are involved. The O_2^* profile given by Huffman et al (1971) is listed in appendix A-1, table A-1-2. Although this O_2^* profile is based on measurements near 70° solar zenith angle, no significant increase in this profile is expected at lower solar zenith angles, on theoretical grounds.

5.3.3 Energetic Particles

We assume that near the magnetic equator precipitated energetic electrons can be neglected as an ionization source for the D- and lower E- region. However we do include in our total Q-function a contribution to galactic cosmic rays. To make this calculation we use an empirical formula (Mitra, 1968) which for magnetic latitudes less than 50° , fits the cosmic ray ionization rates measured by Van Allen (1952).

$$q_{c.r.}(z) = ND(z) \cdot (1.5 \times 10^{-18} \cos^{-4} L_m) \cdot (1 - 3 \times 10^{-3}(F - 70))$$

where ND is the total molecular number density, L_m is magnetic latitude and F is the 10.7 cm solar flux in units of $10^{-22} \text{ W m}^{-2} \text{ Hz}^{-1}$.

5.4 Q-Function Results

At a particular altitude the relative contribution to the total Q function made by a component q_i is a function of solar zenith angle. This is illustrated in Fig. 2 and Fig. 3 which show the q_i components for solar zenith angles of 10° and 60° respectively. Numerical values of our results together with a calculated r.m.s. error on $Q(z)$ are tabulated for four solar zenith angles in appendix A-5.

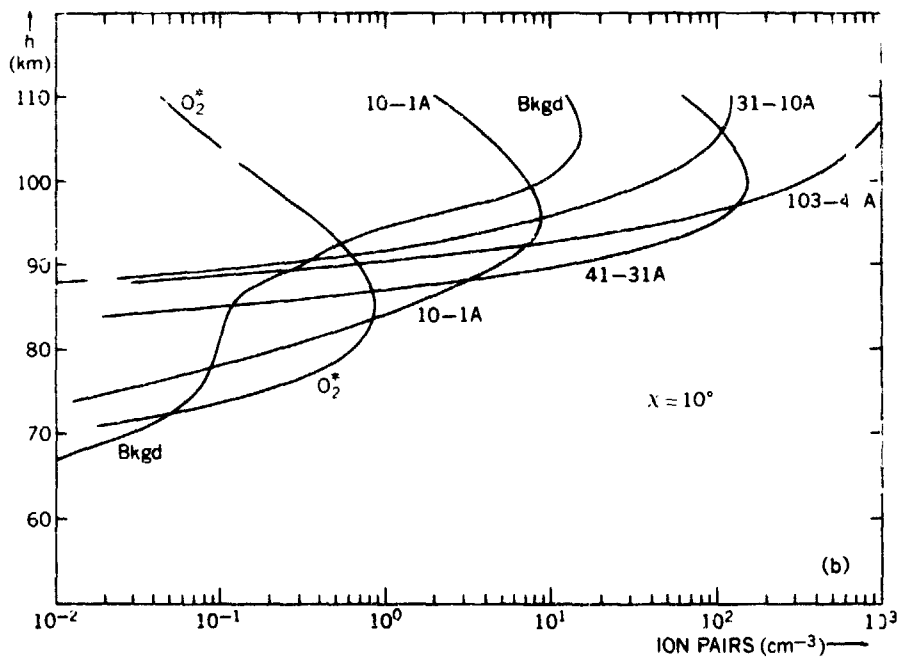
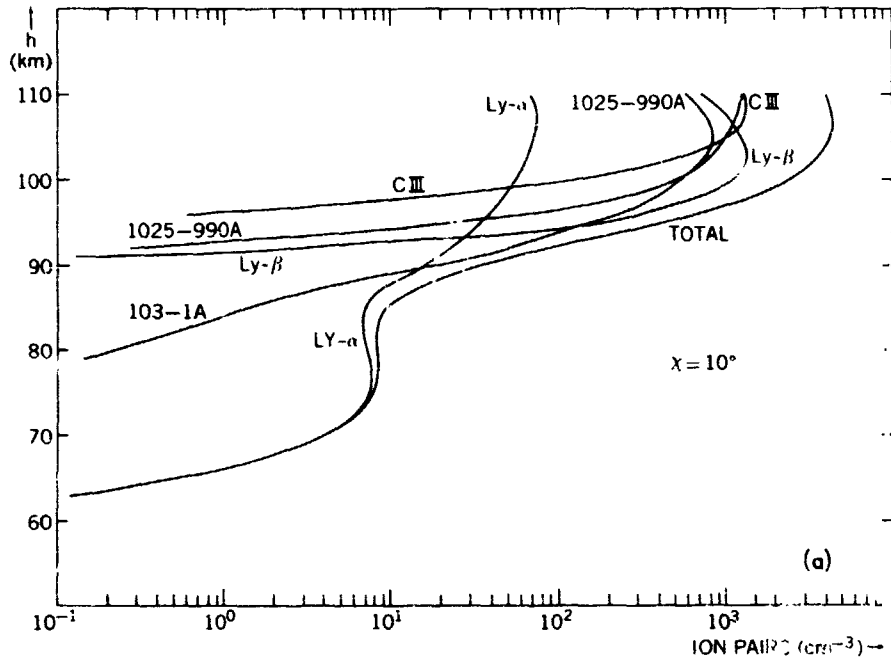


Figure 2. Calculated Q-function and components for $\chi = 10^\circ$.

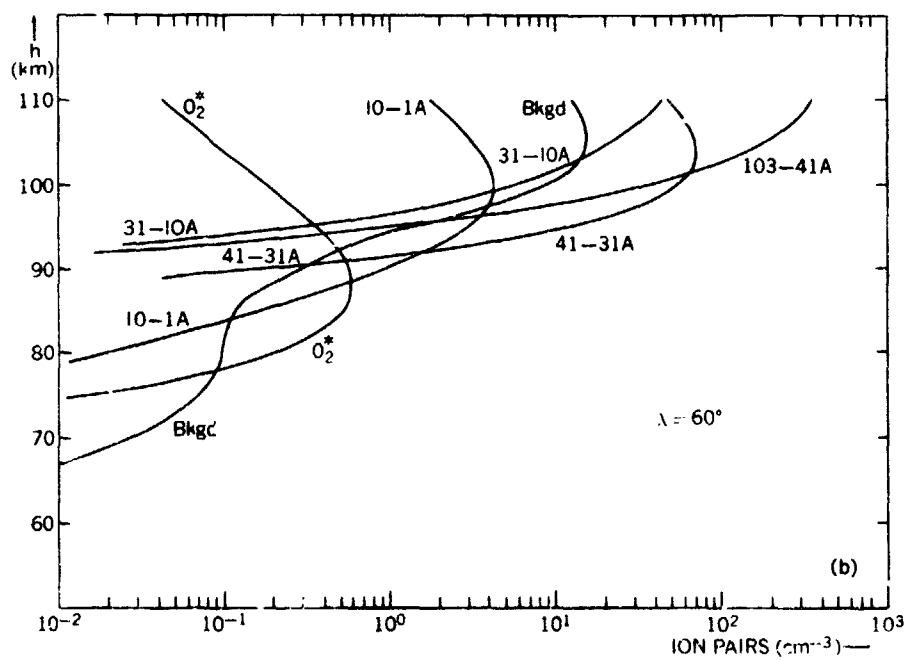
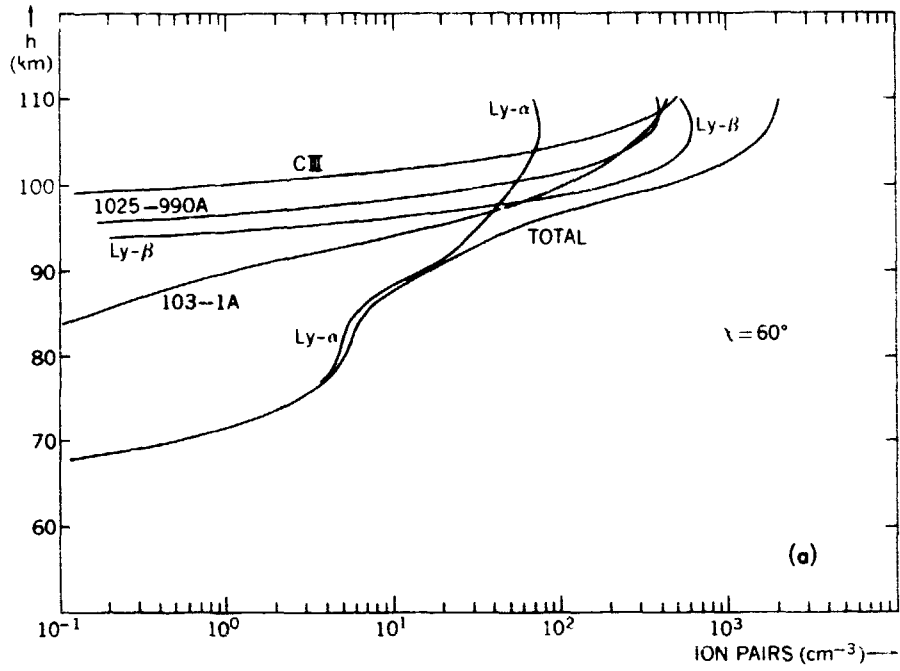


Figure 3. Calculated Q-function and components for $\chi = 60^\circ$.

6. REFERENCE ELECTRON DENSITY PROFILE

The electron density profile has not yet been determined at equatorial latitudes from ground-based methods such as the partial reflection or cross modulation experiment. The few profiles that are available for the equator have been obtained from rocket measurements at Thumba, India (Kane 1969, 1972, Somayajulu et al 1971, Aikin et al 1972). The profile obtained at the smallest solar zenith angle for an undisturbed sun (i.e. 14° , Kane 1969) was adopted as the basis for the 60-82 km segment of our present reference profile. The uppermost portion of our reference profile was determined from empirical formulas which give as a function of solar activity and zenith angle the height and density at the peak of the E-region. In the altitude region between 82 km and the peak of the E-region at 105 km, our reference profile was adjusted by trial and error until calculated values of absorption and virtual height agreed with the extensive multi-frequency absorption and virtual height measurements made at Colombo, Ceylon by Gnanalingam (1972). Details of the procedure for constructing our reference profile are given in appendix A-6. The final profile to emerge from that procedure is shown as the solid curve in Fig. 4. Also shown as the dashed curve in Fig. 4 is an alternate reference profile allowed by the confidence limits on the ground-based measurements. We shall have occasion to refer again to this alternate profile later in section 9.

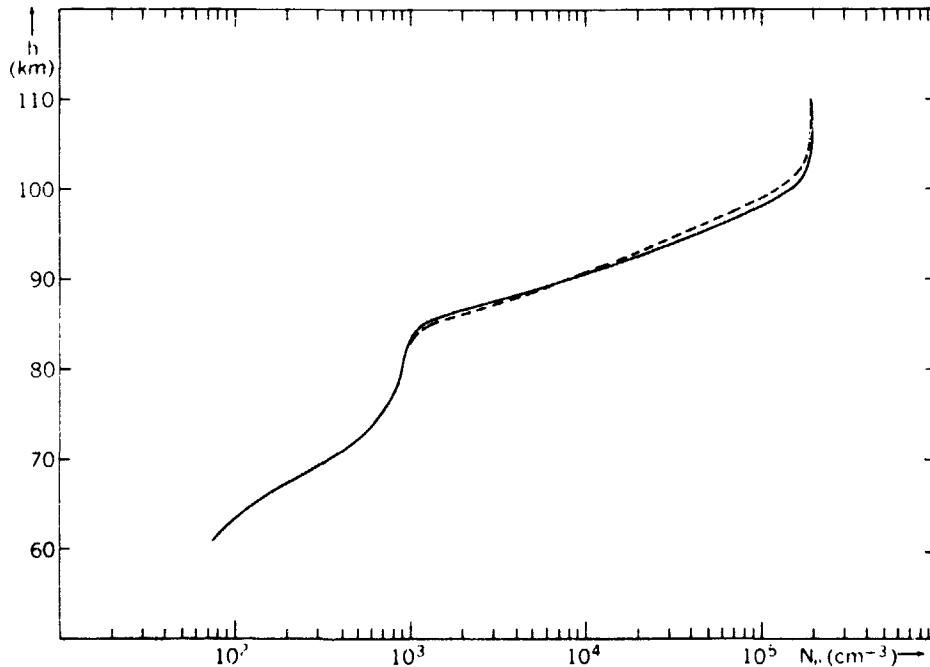


Figure 4. Reference electron density profiles for $\chi = 10^\circ$. Solid curve $N_e(\text{ref})$ is deduced from mean values of multifrequency L, h' measurements (table III), while dashed curve $N_e'(\text{ref})$ is the profile allowed by the upper limit of error on the L, h' measurements.

TABLE III
Model Profile Tested Against 72 Days of Accurate Absorption Measurements

Frequency (MHz)	Virtual Height				Computed Absorption				Computed	
	True Height** (km)	Computed (km)	Measured (km)	60 km to 90 km (db)	90 km to Refl. Level (db)	Phase Integral Correction (db)	Total (db)	Measured Absorption (db)	% Abs. below 90 km	% Abs. below 85 km
1.33*	92.741	96.8	96.5 ± 1.5	48.8	30.8	3.2	82.8	87 ± 6	59%	45%
2.0	95.509	100.4	100.4 ± 1.8	24.8	31.3	1.5	57.6	57.2 ± 2	43%	35%
2.2	96.190	101.3	101.3 ± 1.9	21.2	30.1	1.3	52.6	52.1 ± 2	40%	32%
2.6	97.453	103.0	102.4 ± 2.0	16.0	28.5	1.0	45.5	44.7 ± 2	35%	29%
3.2	99.096	105.4	104.6 ± 2.2	11.2	26.4	0.8	38.4	38.3 ± 2	29%	24%

NOON MEASUREMENTS MADE ON DAYS WHEN THE 1-8A SOLAR X-RAY FLUX WAS LEASS THAN $0.5 \times 10^{-3} \text{ F} \cdot 3 \text{ CM}^{-2} \text{ SEC}^{-1}$ IN THE EQUINOCTIAL MONTHS OF 1968, 1969, 1970. THE MEAN VALUES OF THE RELEVANT SOLAR CONDITIONS WERE: ZENITH ANGLE 10° , SUNSPOT NUMBER 85 AND CM- FLUX 135 UNITS.

* ON 133 MHz, MEASUREMENTS UNDER SIMILAR SOLAR CONDITIONS WERE AVAILABLE FOR ONLY 16 DAYS.

** LEVEL AT WHICH PLASMA FREQUENCY EQUALS EXPLORING WAVE FREQUENCY.

PRECEDING PAGE BLANK NOT FILMED

between α_{eff} and $\bar{\alpha}_d$ in the region below 85 km is to be expected on the basis that our α_{eff} contains a negative ion contribution, i.e.

$$\alpha_{eff} = (1 + \lambda)(\bar{\alpha}_d + \lambda\bar{\alpha}_i) \geq \bar{\alpha}_d$$

where $\bar{\alpha}_i$ is the ion-ion recombination coefficient and $\lambda = N_-/N_e$ is the ratio of negative ion density to electron density. However since definitive values of $\bar{\alpha}_i$ and $\lambda(z)$ are not available, no inference concerning our Q-function or the controlling nitric oxide profile can be drawn from our large values of α_{eff} below 80 km. In the altitude region above 90 km the shape of our α_{eff} profile suggests that here our Q-function is deficient. Either there exists an additional ionization source which we have not taken into account, or we have underestimated one or more of the solar flux components. We shall return to these possibilities later in section 11.

8. ELECTRON DENSITY VERSUS SOLAR ZENITH ANGLE

To obtain the electron density profile as a function of solar zenith angle χ , we numerically solve the following equation:

$$\alpha_{eff} \cdot N_e^2(z, \chi) - Q(z, \chi) - \frac{d}{dt} \{N_e(z, \chi)\}$$

where

$$\alpha_{eff} = Q(10^\circ)/N_e^2(\text{ref}).$$

For $\chi \leq 75^\circ$ we find that the dN/dt term is completely negligible, and that the electron density profile at zenith angle χ is generated from our reference profile according to the expression

$$N_e(z, \chi) = N_e(\text{ref}) \cdot \sqrt{\frac{Q(z, \chi)}{Q(z, 10^\circ)}}.$$

From this relationship it can be seen that the zenith angle dependence of the N_e profile will not be overly sensitive to the absolute values of the solar fluxes since what we are primarily concerned with here are ratios of Q. Calculated N_e profiles for $\chi = 40^\circ, 60^\circ$ and 75° are plotted and discussed in appendix A-7.

Implicit in our construction of the $N_e(z, \chi)$ profiles is the approximation the ratio $\lambda = N_-/N_e$ is time independent (i.e. not a function of solar zenith angle). For the altitudes above 85 km where most of the absorption takes place,

and for solar zenith angles $\chi \leq 75^\circ$, this approximation concerning negative ions should be quite adequate for purposes of calculating radio wave absorption.

9. RADIO WAVE ABSORPTION: CALCULATED VERSUS MEASURED

Having derived the solar zenith angle dependence of N_e by the method described in section 8, we should now be able to predict the diurnal variation in the absorption and the virtual height of reflection of a radio wave vertically incident on the lower ionosphere. In calculating these quantities by means of the generalized magnetoionic ray theory, the electron density and collision frequency profiles were logarithmically interpolated for altitude laminations of 100 meters. However since the complex refractive index changes very rapidly in the region immediately below the height of reflection h_c , the last one kilometer of the calculation was done for laminations of 10 meter thickness. The height of reflection h_c is defined for the ordinary mode as the altitude at which the plasma frequency equals the frequency of the exploring radio wave. To the absorption calculated by ray theory, we add the so called phase integral correction which, near the magnetic equator is relatively small (Thorpe 1971). At our exploring frequencies this combination gives a good approximation to a full wave solution. We estimate that the accuracy on our calculation of absorption is better than ± 1.0 db.

To calculate the virtual height we note that, for an ordinary wave propagating vertically near the magnetic equator, the phase refractive index n and the group refractive index n' are related, to a good approximation, by the expression $nn' = 1$. Hence, from ray theory, the virtual height is given by the integral:

$$h' = \int_0^{h_c} \frac{dz}{n(z)}$$

To this value of virtual height a phase integral correction should be added to give a result closely equivalent to a full wave treatment. Instead however, for ease of computation, we make use of an alternative procedure (Titheridge, 1967) where $n(z)$ in the above integral for h' is evaluated with the collision frequency set equal to zero. We estimate that this procedure yields a virtual height which is accurate to better than ± 0.5 km.

The measured diurnal variation of absorption and virtual height (Gnanalingam, 1972) is given in table IV for the exploring frequencies 2.0 and 2.2 MHz. These results were compiled from measurements on 15 selected days in the equinoctial months of 1968, 1969 and 1970 when the solar conditions met our criteria for an undisturbed sun at solar cycle maximum, (see section 4, table I).

TABLE IV
Measured Absorption and Virtual Height

Frequency (MHz)	Local Time (hours)	χ (deg)	L (db)	δL^* (db)	h' (km)	$\delta h'^*$ (km)
2.2	12:25	7.6	51.8	1.5	102.0	1.1
	13:25	20.3	49.6	1.6	102.2	1.2
	14:25	34.7	47.5	1.5	104.5	1.5
	15:25	49.4	39.0	2.3	107.3	1.1
	16:25	64.3	29.2	2.3	110.3	0.9
	17:25	78.9	20.1	3.8	114.0	4.6
2.0	12:35	10.1	56.4	1.2	101.0	0.8
	13:35	22.7	54.2	1.7	101.1	1.3
	14:35	37.2	51.1	1.7	103.5	1.3
	15:35	51.9	42.4	2.3	106.1	1.4
	16:35	66.8	31.6	2.7	109.1	1.2
	17:35	81.4	21.3	3.8	113.5	3.9

* 95% confidence limit

In Fig. 6 and Fig. 7 the calculated values of absorption and virtual height (shown as circles) are compared with the measured values of Table IV. A striking disagreement between calculation and measurement is immediately obvious. In particular, the calculated virtual height does not increase fast enough as χ increases from 10° to 60° . For χ greater than 60° , the h' increases too steeply in a manner suggestive of group retardation. In the case of absorption, the variation with solar zenith angle seems to agree with measurement up to $\chi = 60^\circ$. However, this must be considered fortuitous because the same N_e profiles do not yield the observed h' - χ dependence. At χ values greater than 60° , the peculiar variation of absorption is a direct consequence of the too rapid increase in the h' value. A consideration of these discrepancies indicates that at altitudes above 95 km our N_e values do not decrease fast enough with solar zenith angle.

In the above analysis with $N_e(z, \chi)$ profiles have been generated from what should be regarded as the most probable N_e (ref) profile, because it is this profile which is most consistent with the mean values of the multi-frequency L, h' measurements made at $\chi = 10^\circ$. It is clear however that we could have constructed other N_e (ref) profiles which are consistent with the confidence limits of the measurements. We therefore consider the possibility that by starting from a different N_e (ref) profile we can generate a set of $N_e(z, \chi)$ values which yield better agreement with the measured diurnal variations. However, by trial and error, the best we could do along these lines is shown by the crosses of Fig. 6.

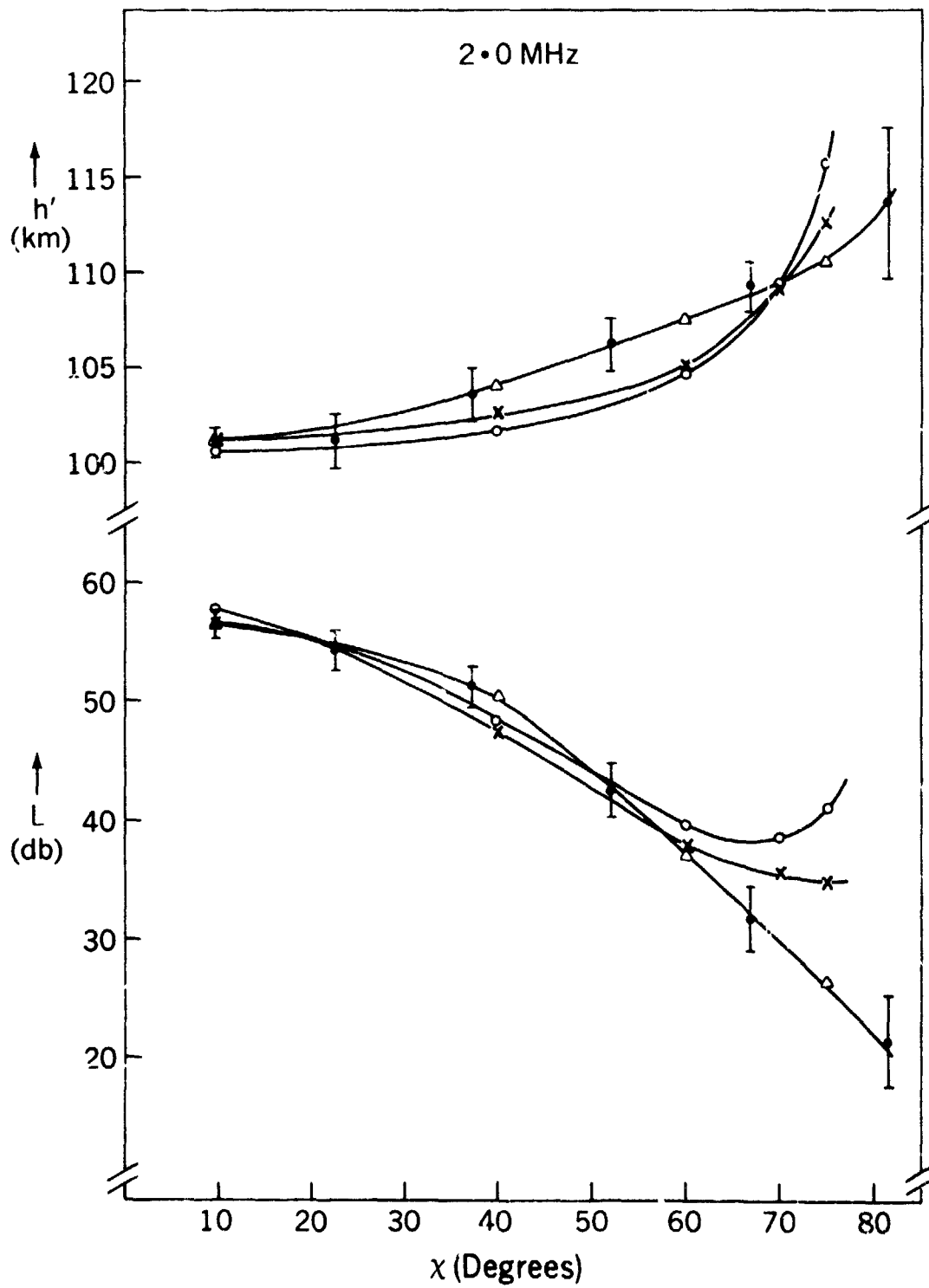


Figure 6. 2.0 MHz absorption and virtual height: calculated versus measured. Measured values are given with error bars

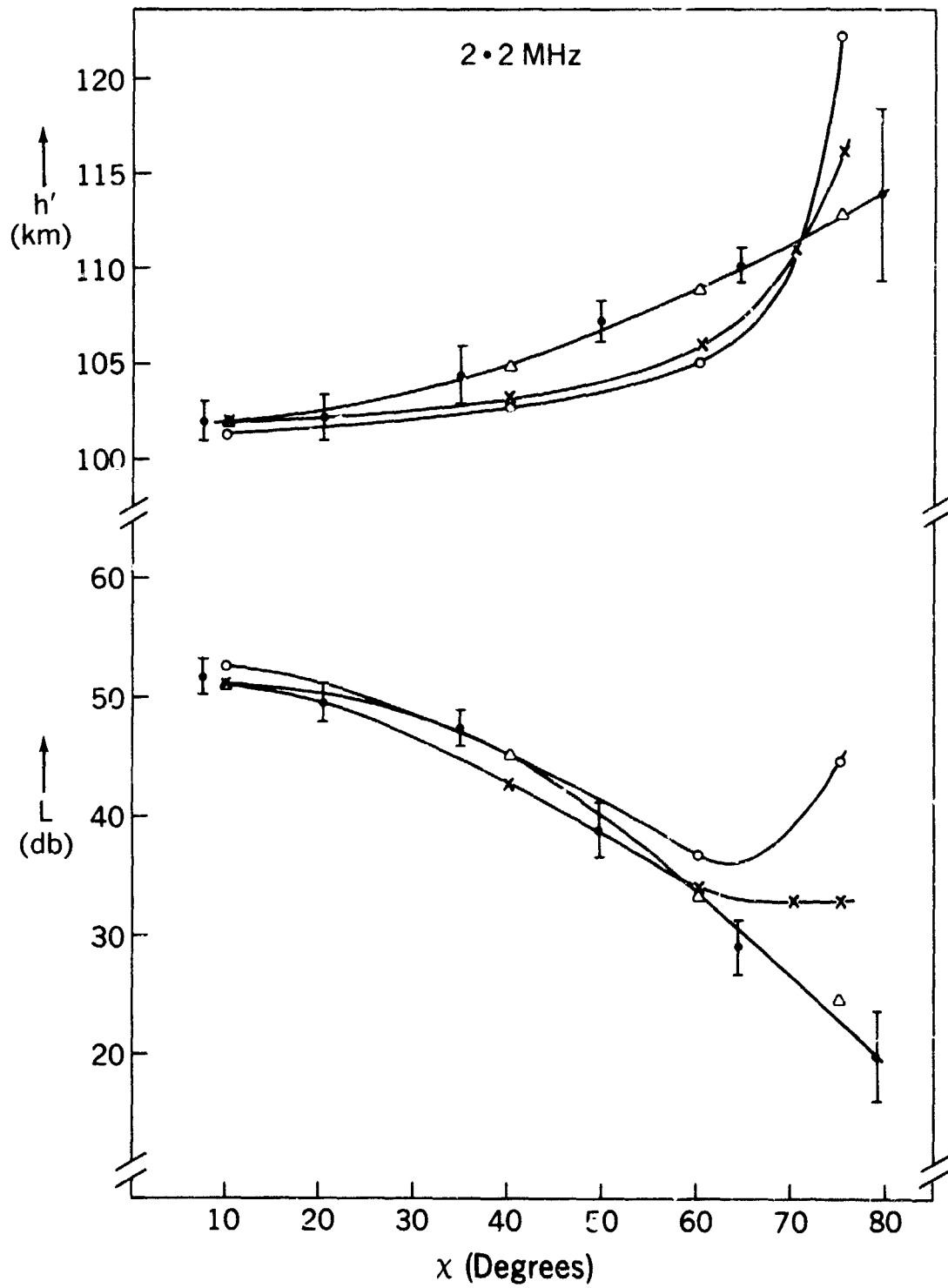


Figure 7. 2.2 MHz absorption and virtual height: calculated versus measured. Measured values are given with error bars.

The corresponding electron density profile is that labelled $N'(\text{ref})$ in Fig. 4, previously referred to in section 6. In Fig. 6 it will be noted that even with the most favorable reference profile $N'(\text{ref})$ we can get marginal agreement between calculated and measured L, h' only out to $\chi = 40^\circ$ on the basis of our present knowledge of the Q -functions. The apparent agreement in h' at $\chi = 70^\circ \sim 75^\circ$ is fortuitous, being merely the intersection of two dissimilar variations, one calculated and the other measured.

For the sake of completeness, however, it is of interest to find a set of electron density profiles which do yield agreement with the $L, h'(\chi)$ measurements. This we do in the following section, even though we are unable to generate such profiles from our present understanding of the Q -functions. The calculated values of $L, h'(\chi)$ resulting from these ad-hoc profiles are shown as the triangular points in Fig. 6 and 7.

10. $N_e(z, \chi)$ MODEL FOR THE LOWER EQUATORIAL IONOSPHERE AT EQUINOX

We have already drawn attention to the fact that our present approach, based on our knowledge of the Q -functions, is only marginally adequate to generate N_e profiles that are consistent with the measured diurnal variations up to $\chi = 40^\circ$. At this zenith angle the highest altitude which enters into our analysis is the true height of reflection on 2.2 MHz (i.e. 98.2 km). It would therefore seem that the N_e profiles need to be modified only at altitudes above 98.2 km. However, to get better agreement with the measurements we find that the modification should begin at about 95 km. It is interesting to note that this is the level at which the slope of the α_{eff} profile begins to depart noticeably from the slope of the $\bar{\alpha}_d$ profile (Fig. 5). In modifying the profiles above 95 km we are constrained by the well-established relationships concerning the zenith angle dependence of foE and $h_m E$ (see Appendix A-6). The final profiles to emerge from these modifications are tabulated in appendix A-8 and plotted in Fig. 8.

An interesting feature predicted by our equatorial $N_e(\chi)$ model is the relatively small χ dependence of electron density in the 85-90 km altitude interval. A test of this prediction, which could be a fairly simple ground-based experiment, would be very helpful at this stage. Also shown in Fig. 8 by the dashed curves are the inadequate N_e profiles generated by the Q -functions. Significant differences between the two sets of profiles are immediately evident. The question naturally arises whether these differences could tell us something about the shortcomings in our theory of ion-production and loss.

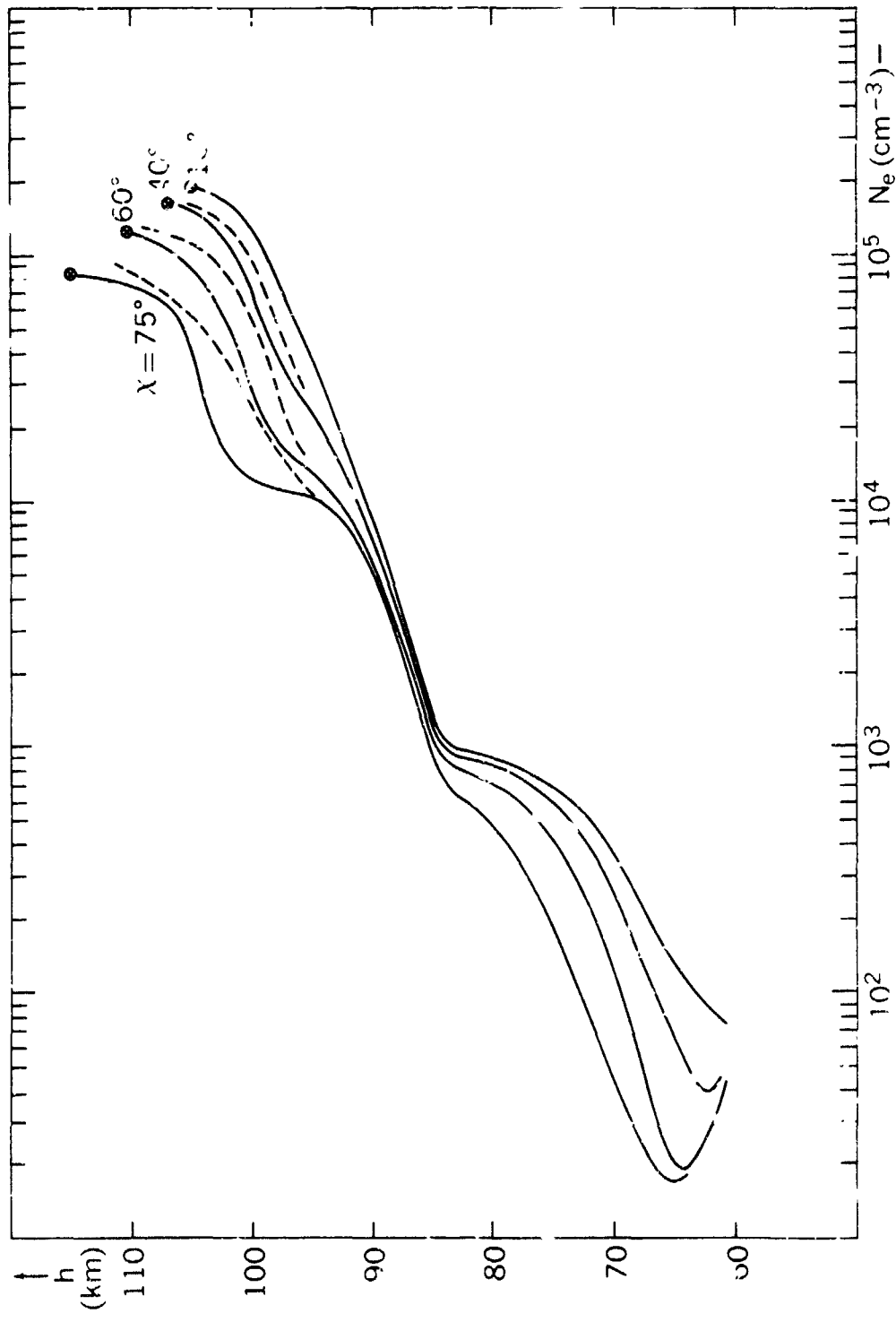


Figure 8. Ad hoc model of solar zenith angle dependence of the equatorial e^- coron density profile. The solid curves are the profiles required to match the measurements of absorption and virtual height, while the dashed curves are the inadequate profiles calculated from our knowledge of the Q-function behavior.

11. DISCUSSION AND CONCLUSION

In attempting to answer the above question we note that α_{eff} (Fig. 5) is substantially less than $\bar{\alpha}_d$ at all altitudes above 90 km. This would seem to indicate that there is a component missing from our Q-function. Given the correct set of N_e profiles (Fig. 8) and assuming $\alpha_{eff} \equiv \bar{\alpha}_d$ above 90 km, we could deduce such a missing component. However, when we do this we find that the missing Q component decreases with solar zenith angle much faster than the decrease associated with a photon source. This must mean either that ionization sources other than solar photons and/or that loss processes other than simple recombination are operative at the 100 km level in the equatorial ionosphere.

Clearly the problem deserves consideration beyond what has been attempted in the present paper. Until it is resolved, our understanding of the basic processes of the lower ionosphere will continue to be in doubt.

APPENDIX A-1

Atmospheric Model

The time independent atmospheric model which is used throughout the present work is based on the lower altitude data of Groves (1971) for 10° latitude at equinox, and extrapolated to 160 km by means of the Jacchia (1971) model for an exospheric temperature of 1100 degrees Kelvin. In column 2 of table A-1-1, M is the gram molecular weight taken from Jacchia. The temperatures, pressures and mass densities from Groves are given in columns 3, 4 and 5. The number density ND is computed from the relation $ND = (MD \times 10^{-3}) \times (6.023E23) \times M$, and is listed in column 6. (6.023E23 is Avogadro's number). Below 90 km the molecular nitrogen density in column 7 is given by $N_2 = 0.7811 \times ND$, while the molecular oxygen density in column 8 is given by $O_2 = 0.20955 \times ND$. At the altitudes 90 and 95 km the percentage of N_2 and O_2 is given in the footnote at the bottom of the table. For the altitude region of 100 to 160 km the N_2 , O_2 and O densities are taken from the Jacchia tables but enhanced by a factor of 1.1727. The factor of 1.1727 is necessary to normalize the Jacchia densities to the data of Groves in the overlapping altitude range of 95 to 110 km.

In table A-1-2 we give the logarithmically interpolated values of our atmospheric model for the altitude region between 60 and 110 km. Included in table A-1-2 are models of two minor constituents, nitric oxide and metastable oxygen $O_2^* (^1\Delta_g)$. The nitric oxide model is taken from the measurements of Meira (1970), while the O_2^* values are those given by Huffman et al (1971).

TABLE A-1-i

z (km)	M (gram)	T (deg)	P (mks)	MD (mks)	ND (cgs)	N ₂ (cgs)	O ₂ (cgs)	O (cgs)
25	28.96	221	250(1)	394(-4)	819(15)	640(15)	172(15)	
30	28.96	233	119(1)	178(-4)	370(15)	289(15)	776(14)	
35	28.96	249	588(0)	823(-5)	171(15)	134(15)	359(14)	
40	28.96	262	306(0)	406(-5)	844(14)	660(14)	177(14)	
45	28.96	272	162(0)	208(-5)	433(14)	338(14)	907(13)	
50	28.96	274	883(-1)	112(-5)	233(14)	182(14)	488(13)	
55	28.96	265	473(-1)	622(-6)	129(14)	101(14)	271(13)	
60	28.96	246	247(-1)	350(-6)	728(13)	569(13)	153(13)	
65	28.96	227	121(-1)	186(-6)	387(13)	302(13)	811(12)	
70	28.96	210	568(-2)	942(-7)	196(13)	153(13)	411(12)	
75	28.96	200	250(-2)	435(-7)	905(12)	707(12)	190(12)	
80	28.96	199	109(-2)	190(-7)	395(12)	309(12)	828(11)	
85	28.95	200	471(-3)	821(-8)	171(12)	133(12)	358(11)	
90*	28.83	197	206(-3)	364(-8)	760(11)	597(11)	157(11)	779(9)
95**	28.23	193	880(-4)	157(-8)	335(11)	258(11)	606(10)	169(10)
100		201	386(-4)			105(11)	217(10)	128(10)
105		229	182(-4)			433(10)	803(9)	742(9)
110		278	980(-5)			188(10)	315(9)	434(9)
115						879(9)	136(9)	262(9)
120						449(9)	644(8)	166(9)
125						250(9)	338(8)	111(9)
130						151(9)	193(8)	786(8)
135						970(8)	119(8)	581(8)
140						657(8)	771(7)	446(8)
145						464(8)	524(7)	353(8)
150						338(8)	369(7)	286(8)
155						254(8)	268(7)	236(8)
160						194(8)	199(7)	199(8)

* at z = 90 km N₂ = 0.7848 × ND; O₂ = 0.2059 × ND

** at z = 95 km N₂ = 0.7694 × ND; O₂ = 0.1809 × ND

TABLE A-1-2
Atmospheric Model

z (km)	O (cm ³)	O ₂ (cm ³)	N ₂ (cm ³)	NO (cm ³)	O ₂ ⁺ (cm ³)
6.000E1		1.527E15	5.686E15	2.600E8	1.658E10
6.100E1		1.347E15	5.010E15	2.280E8	1.531E10
6.200E1		1.175E15	4.415E15	2.000E8	1.414E10
6.300E1		1.044E15	3.891E15	1.730E8	1.307E10
6.400E1		9.199E14	3.429E15	1.520E8	1.207E10
6.500E1		8.106E14	3.022E15	1.320E8	1.115E10
6.600E1		7.075E14	2.637E15	1.150E8	1.030E10
6.700E1		6.175E14	2.302E15	1.050E8	9.514E9
6.800E1		5.387E14	2.009E15	8.800E7	8.739E9
6.900E1		4.704E14	1.753E15	7.700E7	8.119E9
7.000E1		4.105E14	1.530E15	6.800E7	7.500E9
7.100E1		3.583E14	1.311E15	5.850E7	6.928E9
7.200E1		3.014E14	1.123E15	5.100E7	6.405E9
7.300E1		2.587E14	9.626E14	4.450E7	5.879E9
7.400E1		2.217E14	8.248E14	3.900E7	5.400E9
7.500E1		1.896E14	7.067E14	3.370E7	5.144E9
7.600E1		1.606E14	5.988E14	2.930E7	4.700E9
7.700E1		1.361E14	5.074E14	2.600E7	4.590E9
7.800E1		1.153E14	4.299E14	2.280E7	4.300E9
7.900E1		9.772E13	3.643E14	2.030E7	4.042E9
8.000E1		8.280E13	3.087E14	1.800E7	3.800E9
8.100E1		7.002E13	2.610E14	1.640E7	3.541E9
8.200E1		5.920E13	2.207E14	1.500E7	3.300E9
8.300E1		5.006E13	1.866E14	1.400E7	3.040E9
8.400E1		4.233E13	1.578E14	1.340E7	2.800E9
8.500E1		3.579E13	1.334E14	1.350E7	2.565E9
8.600E1		3.034E13	1.136E14	1.410E7	2.350E9
8.700E1		2.571E13	9.671E13	1.550E7	2.113E9
8.800E1		2.179E13	8.233E13	1.800E7	1.900E9
8.900E1		1.847E13	7.010E13	2.250E7	1.688E9
9.000E1	7.793E11	1.566E13	5.968E13	2.830E7	1.500E9
9.100E1	9.101E11	1.295E13	5.045E13	3.320E7	1.342E9
9.200E1	1.063E12	1.071E13	4.265E13	3.820E7	1.200E9
9.300E1	1.241E12	8.858E12	3.606E13	4.330E7	1.028E9
9.400E1	1.449E12	7.327E12	3.049E13	4.900E7	8.800E8
9.500E1	1.693E12	6.060E12	2.577E13	5.450E7	7.563E8
9.600E1	1.601E12	4.934E12	2.152E13	6.050E7	6.500E8
9.700E1	1.514E12	4.018E12	1.798E13	6.700E7	5.586E8
9.800E1	1.432E12	3.272E12	1.501E13	7.400E7	4.800E8
9.900E1	1.354E12	2.664E12	1.254E13	8.100E7	4.040E8
1.000E2	1.281E12	2.169E12	1.047E13	9.000E7	3.400E8
1.010E2	1.148E12	1.778E12	8.779E12	9.500E7	2.915E8
1.020E2	1.029E12	1.457E12	7.358E12	1.000E8	2.500E8
1.030E2	9.228E11	1.195E12	6.167E12	1.040E8	2.179E8
1.040E2	8.273E11	9.793E11	5.169E12	1.090E8	1.900E8
1.050E2	7.416E11	8.028E11	4.333E12	1.120E8	1.631E8
1.060E2	6.662E11	6.659E11	3.666E12	1.150E8	1.400E8
1.070E2	5.984E11	5.523E11	3.102E12	1.180E8	1.183E8
1.080E2	5.375E11	4.581E11	2.625E12	1.180E8	1.000E8
1.090E2	4.828E11	3.800E11	2.221E12	1.130E8	9.055E7
1.100E2	4.337E11	3.152E11	1.879E12	1.100E8	8.200E7

APPENDIX A-2

Electron Collision Frequency Model

Throughout the present work the electron collision frequency is assumed to be independent of solar zenith angle. The total collision frequency $\nu = \nu_p + \nu_{ei} + \nu_{eo}$ and its components are listed below. ν_p is the component due to electron collisions with O_2 and N_2 molecules, ν_{ei} is the component due to Coulomb collisions, and ν_{eo} is the component due to electron-atomic oxygen collisions.

PRECEDING PAGE BLANK NOT FILMED

TABLE A-2-1
Collision Frequency

z (km)	ρ (sec ⁻¹)	ρ_{co} (sec ⁻¹)	ρ_{co} (sec ⁻¹)	ρ_{co} (sec ⁻¹)
60	1.606E7			1.606E7
61	1.392E7			1.392E7
62	1.207E7			1.207E7
63	1.046E7			1.046E7
64	9.072E6			9.072E6
65	7.865E6			7.865E6
66	6.761E6			6.761E6
67	5.812E6			5.812E6
68	4.996E6			4.996E6
69	4.295E6			4.295E6
70	3.692E6			3.692E6
71	3.133E6			3.133E6
72	2.679E6			2.659E6
73	2.256E6			2.256E6
74	1.915E6			1.915E6
75	1.625E6			1.625E6
76	1.376E6			1.376E6
77	1.166E6			1.166E6
78	9.975E5			9.875E5
79	8.365E5			8.365E5
80	7.085E5			7.085E5
81	5.990E5			5.990E5
82	5.065E5			5.065E5
83	4.282E5			4.282E5
84	3.621E5			3.621E5
85	3.062E5			3.062E5
86	2.595E5			2.595E5
87	2.199E5			2.199E5
88	1.864E5			1.864E5
89	1.580E5			1.580E5
90	1.339E5	2.060E3	1.469E2	1.361E5
91	1.130E5	2.400E3	1.307E2	1.155E5
92	9.529E4	2.796E3	2.476E2	9.833E4
93	8.038E4	3.257E3	3.215E2	8.396E4
94	6.781E4	3.794E3	4.173E2	7.202E4
95	5.720E4	4.420E3	5.418E2	6.216E4
96	4.851E4	4.197E3	6.718E2	5.338E4
97	4.114E4	3.984E3	8.329E2	4.595E4
98	3.489E4	3.783E3	1.033E3	3.970E4
99	2.959E4	3.592E3	1.280E3	3.446E4
100	2.509E4	3.410E3	1.587E3	3.009E4
101	2.159E4	3.098E3	1.698E3	2.638E4
102	1.857E4	2.814E3	1.816E3	2.320E4
103	1.598E4	2.557E3	1.942E3	2.048E4
104	1.375E4	2.323E3	2.076E3	1.815E4
105	1.183E4	2.110E3	2.221E3	1.616E4
106	1.045E4	1.930E3	2.105E3	1.449E4
107	9.235E3	1.765E3	1.996E3	1.300E4
108	8.160E3	1.614E3	1.892E3	1.167E4
109	7.210E3	1.476E3	1.794E3	1.048E4
110	6.370E3	1.350E3	1.700E3	9.420E3

APPENDIX A-3

Solar Radiations

HYDROGEN LYMAN- α (1215.7A) AND LYMAN- β (1205.7A)

Intensity measurements of the solar Lyman- α and Lyman- β emission lines made at different levels of solar activity are reviewed in Tables A-2.1 and A-2.2 respectively. Also included in the tables are the average 10.7 cm solar flux values for the dates of these measurements.

For the present work we need to know the mean intensities of these lines at a typical solar cycle maximum when the 10.7 cm flux lies in the range $130-160 \times 10^{-22} \text{ Wm}^{-2} \text{ Hz}^{-1}$ (flux unit). In the case of the Lyman- α line, there are only a few reliable measurements reported for these solar maximum conditions. However, several measurements are available for the solar minimum period 1964/65 (Weeks 1967). In order to derive from the latter measurements a representative value of the intensity at solar maximum we examine the solar-cycle variation of both the Lyman- α and Lyman- β intensities.

Inspection of the tables will show that, while there is a general increase in the intensities of these lines with solar activity, the scatter in the measurements, especially of the Lyman- β line, makes it difficult to evaluate the magnitude of this increase. A study of the solar-cycle variation of the sum of the intensities of several chromospheric emission lines, including Lyman- β , has indicated an increase of the EUV flux by a factor of 1.5 for an increase in the 10.7 cm flux by a factor 2, from 75 to 150 units (Hall et al 1969). These intensities were derived from rocket-borne measurements carried out during the period from August 1961 to November 1968. A similar relationship has been noted in the measurements made by a spectrometer aboard the satellite OSO 3 during a solar rotational period of 27 days in May 1967 when the opposite hemispheres of the sun exhibited very different levels of solar activity. The intensities of the Lyman- α and Lyman- β lines were observed to increase by factors of 1.3 and 1.4 respectively when the 10.7 cm flux increased from 111 units to 201 units (Hall and Hinteregger 1970). These factors have an accuracy of approximately ± 0.1 . Having regard to all the available observations, we estimate the solar-cycle factor to be 1.4 for both these lines.

Applying this factor to the average value of the Lyman- α intensity at solar cycle minimum, which we estimate to be $3.9 \text{ ergs cm}^{-2} \text{ sec}^{-1}$ from Table A-2.1

(after excluding extreme values), we obtain a figure of $5.4 \text{ ergs cm}^{-2} \text{ sec}^{-1}$ or $3.3 \times 10^{11} \text{ ph cm}^{-2} \text{ sec}^{-1}$ for the intensity at a typical solar cycle maximum. This figure is rather less than the value of 6.1 ± 0.45 deduced by Weeks (1967) for solar maximum, because his average value is weighted by the measurements made during the period of unusual solar activity in 1957/58.

The mean intensity of the Lyman- β line may be deduced directly from Table A-2.2 which contains an adequate number of measurements corresponding to this range of 10.7 cm flux. It is found to be $3.6 \times 10^9 \text{ ph cm}^{-2} \text{ sec}^{-1}$ or $7.0 \times 10^{-2} \text{ erg cm}^{-2} \text{ sec}^{-1}$.

THE CONTINUUM 1025-990 A

Hinteregger et al (1965) report a value of $2.7 \times 10^9 \text{ cm}^{-2} \text{ sec}^{-1}$ for the photon flux in this wavelength band at solar minimum conditions. By normalizing this value to the adjacent 1025.7A Lyman- β flux also reported by Hinteregger et al for solar minimum, we obtain $4.2 \times 10^9 \text{ cm}^{-2} \text{ sec}^{-1}$ for the value of photon flux that is used in the present paper.

THE CARBON III LINE AT 977 A

Published values of the intensity of this solar emission line measured by rocket- and satellite-experiments are to be found in Hall et al (1969) and Hall and Hinteregger (1970). For an undisturbed sun at solar cycle maximum we adopt the value of $4.4 \times 10^9 \text{ ph cm}^{-2} \text{ sec}^{-1}$ ($9.0 \times 10^{-2} \text{ erg cm}^{-2} \text{ sec}^{-1}$) recommended by Hinteregger (1970) in his review of the EUV solar spectrum.

X-RAYS IN THE WAVELENGTH RANGE 100-1A

For aeronomical calculations it is informative to divide this wavelength range into several X-ray bands which deposit their energy at different altitudes in the lower ionosphere.

100-40A and 30-10A

These bands are characterized by the presence of a number of spectral lines which have been investigated in some detail because of their importance in the study of solar physics. The greater part of the ionization produced by these bands occurs in the altitude range 95-120 km, when the solar zenith angle is small.

The flux in the bands 8-20A and 44-60A has been systematically monitored for a number of years by ion chambers on board the NRL SOLRAD satellites. Of the two bands, both of which produce a peak of ionization around 103 km ($\chi = 10^\circ$), the 44-60A band is the more important from the point of view of E-region formation.

The published flux data in this band have generally been derived from the ion-chamber currents on the assumption that the incident solar radiation may be represented approximately by a gray-body distribution at a temperature of 0.5×10^6 °K (Kreplin 1961). Since the actual spectrum is marked by several lines, the published data are subject to some error. Even more serious is the fact that the 44-60A photometers employed in the SOLRAD satellites respond with high efficiency to X-radiation of wavelength less than 20A (Kreplin and Horan 1969: NRL Report 6800, p. 39). Although the contribution to the photometer output from this radiation is relatively small when the sun is quiet, it is appreciable at solar maximum and frequently dominates the output during solar flares (Kreplin and Gregory 1966). The true values of the flux at solar maximum are probably much less than the uncorrected published data, which lie in the range $0.1-0.6$ erg cm^{-2} sec^{-1} for a non-flaring sun.

Spectrometric measurements of the line intensities and continuum in this band (Manson 1967, 1968; Hinteregger 1970) have yielded integrated flux values that are significantly less than the SOLRAD data. Typical fluxes are 0.021 and 0.030 erg cm^{-2} sec^{-1} for the 40-50A and 50-60A bands respectively. In the present paper we have adopted the measurements given in a recent review by Manson (1972). Any systematic error in the calibration of the instruments from which these measurements were obtained has been estimated by him to be within $\pm 25\%$.

40-30A

Solar radiation in this band is the principal source of daytime ionization at altitudes around 90 km. Since the major part of the noon absorption of radio waves of frequency 1.5 - 2.5 MHz occurs at these altitudes, the 30-40A band of the solar spectrum is of particular importance in the interpretation of absorption measurements. Unfortunately the flux in the band has not yet been systematically monitored by detectors aboard satellites.

Our present knowledge of this flux is mainly based on a few measurements made with rocket-borne instruments, of the intensities of individual spectral lines within the band. The most prominent of these lines is the CVI line at 33.7A. Published measurements of the intensity of this line are shown in Table A-2.3. It will be noted that there is an inconsistency in the measurements.

For the same level of solar activity, as indicated by the 10.7 cm flux, the values differ by a wide margin, in some instances by nearly an order of magnitude.

The reasons for these discrepancies have not been resolved. In a search for an explanation Manson (1972) has examined the solar conditions that prevailed during each of several measurements carried out by the AFCRL group, the NRL group and the Culham group (Freeman and Jones 1970). His conclusion is that each high value of intensity reported and each remarkably strong image on a photographic spectrum which has been published for this line can be explained by flaring or 'near-Flaring' conditions. This line was only marginally detected when the solar spectrum was sampled under non-flaring conditions on 8 August 1967 (10.7 cm flux = 143 units): and the background level was too high to allow a meaningful integrated flux to be reported for the 30-40A band (Manson 1972). We have therefore adopted a value that is slightly higher than the flux reported by Manson for solar minimum. This value is also consistent with the flux in the neighbouring bands (see Figure 1).

Wavelengths Less than 10A

X-rays of wavelength less than 10A produce a peak of ionization at an altitude of about 95 km ($\chi = 10^{\circ}$) when the sun is quiet, and at progressively lower altitudes as the hardness of the X-ray spectrum increases with solar activity.

The flux in several bands in this short wavelength 'tail' of the solar spectrum has been systematically monitored for several years with instruments on board satellites. The 1-10A flux values adopted by us are based on the SOLARD 9 data. The reduced data are published in the solar Geophysical Data Bulletins as hourly averages of the flux in the bands 1-8A and 8-20A. They are also available in the form of minute-by-minute listings for these bands as well as the 0.5 - 3A band, upon request to the NRL. A noteworthy feature of the measurements is that there is provision of the effects of particle interference on the ion chambers to be detected and filtered out of the measurements in the data reduction process (Kreplin and Horan 1969).

In applying the data to aeronomical calculations it is important to remember that the fluxes are derived by using a gray-body spectrum. The assumed temperature is 2×10^6 K for the 1-8A detector and 10^7 K for the 0.5-3A detector. Horan (1970) has re-evaluated the detector-current to energy-flux conversion constants for these detectors on the basis of a bremsstrahlung-type emission spectrum at different temperatures. The values obtained by him for the 1-8A detector are consistently less than the conversion constant derived from a gray-body spectrum at 2×10^6 K. Bremsstrahlung-type distributions at 3.5×10^6 K and 7.0×10^6 K give constants that are respectively 18% and a

factor of two less than the assumed value. Similarly, the constant for the 0.5-3A detector is 3-13% less than the assumed value, for temperatures in the range $7-20 \times 10^6$ K. Horan (1970) has also shown how the temperature of the X-ray emitting regions, assumed to be isothermal, may be deduced from the ratio of the fluxes in the 1-8A and 0.5-3A bands.

In the present work we have been unable to derive this temperature for an undisturbed sun, using the method suggested by Horan, because measurements of the 0.5-3A flux are not available for these solar conditions. The flux in this band from a non-flaring sun is generally below the SOLRAD 9 detector threshold even at sunspot maximum. We have therefore had to rely on estimates of the temperature obtained from other experiments (Neupert 1969, Pounds 1970) and have adopted a temperature of 3.5×10^6 K for the undisturbed sun at solar cycle maximum. The flux values have been calculated at 1A intervals by fitting a bremsstrahlung-type spectrum at this temperature to the SOLRAD 9 measurement of 4×10^{-4} erg cm⁻² sec⁻¹ for the average 1-8A energy flux under these solar conditions.

For the moderately disturbed sun to be considered in a later Part II of this work the 1-8A flux lies in the range $2.0-2.5 \times 10^{-3}$ erg.cm⁻² sec⁻¹. Even at this level of solar activity the 0.5-3A flux is barely measurable by the SOLRAD 9 detectors. However, by examining a large number of minute-by-minute listings of the fluxes in the 0.5-3A and 1-8A bands, we have estimated the temperature of the X-ray active regions to be 7.0×10^6 K.

Table A-3.1
Solar Lyman- α Measurements

Date	Lyman- α Flux		Reference
	10.7 cm Flux ($10^{-22} \text{ W m}^{-2} \text{ Hz}^{-1}$)	($10^{11} \text{ ph cm}^2 \text{ sec}^{-1}$)	
18 Oct. 1955	85	5.7(-1+3)	Byram et al. (1956)
21 Oct. 1955	94	4.0(± 0.8)	Byram et al. (1956)
4 Nov. 1955	116	9.2(± 3.0)	Byram et al. (1956)
20 July 1956	144	6.1(± 0.5)	Chubb et al. (1957)
25 July 1956	170	6.7(± 0.3)	Chubb et al. (1957)
29 July 1957	201	6.1(± 0.3)	Byram et al. (1958)
23 Mar. 1958	268	6.3(± 0.3)	Byram et al. (1958)
19 Apr. 1960	170	6.0	Detwiler et al. (1961)
19 Aug. 1960	234	5-6	Yefremov et al. (1963)
21 June 1961	132	4.9	Tousey (1964)
23 Aug. 1961	98	5.1	Hall, Schweizer and Hinteregger (1965)
22 Aug. 1962	80	3.5	Tousey (1964)
8 Mar. 1963	83	4.9(± 1.6)	Aikin, Kane & Troim (1964)
9 Apr. 1963	82	4.9(± 1.6)	Aikin, Kane & Troim (1964)
10 July 1963	86	4.4	Hinteregger, Hall and Schmidtke (1965)
6 Dec. 1963	76	5.4	Carver et al. (1964)
12 Dec. 1963	82	4.4	Hall, Schweizer and Hinteregger (1965)
15 July 1964	72	3.5, 3.7(± 15)	Weeks (1967)

Table A-3.1 (Continued)
Solar Lyman- α Measurements

Date	10.7 cm Flux	Lyman- α Flux		Reference
	(10^{-22} Wm $^{-2}$ Hz $^{-1}$)	(ergs cm $^{-2}$ sec $^{-1}$)	(10^{11} ph cm $^{-2}$ sec $^{-1}$)	
19 Nov. 1964	73	4.2(\pm 15%)	2.6	Weeks (1967)
9 Apr. 1965	72	3.9(\pm 15%)	2.4	Weeks (1967)
14 June 1965	79	6.4(\pm 15%)	3.9	Weeks (1967)
17 June 1965	79	3.7(\pm 15%)	2.3	Weeks (1967)
15 Sep. 1965	76	5.9(\pm 15%)	3.5	Weeks (1967)
15 Dec. 1965	74	4.6(\pm 15%)	2.8	Weeks (1967)
14 Apr. 1966	91	5.2	3.2	Bruner and Parker (1966)
14 June 1966	97	4.9(\pm 15%)	3.0	Weeks (1967)
11 Mar. 1967	142	5.0	3.1	Hall & Hinteregger (1970)

Table A-3.2
Solar Lyman- β Measurements

Date	10.7 cm Flux		Lyman- β Flux		
	$(10^{-22} \text{ W m}^{-2} \text{ Hz}^{-1})$	$(\text{ergs cm}^{-2} \text{ sec}^{-1})$	$(10^9 \text{ ph cm}^{-2} \text{ sec}^{-1})$		
23 Aug. 1961	98	0.048	2.5	Hill et al. (1969)	
5 June 1962	85	0.050	2.6	Hill et al. (1969)	
10 July 1963	86	0.045	2.3	Hinteregger, Hill and Schmidke (1965)	
12 Dec. 1963	82	0.035	1.8	Hill et al. (1969)	
12 Aug. 1965	78	0.068	3.5	Hill et al. (1969)	
9 Nov. 1965	80	0.039	2.0	Hill et al. (1969)	
30 Mar. 1966	99	0.054	2.8	Hill et al. (1969)	
22 July 1966	107	0.062	3.2	Hill et al. (1969)	
26 Aug. 1966	130	0.072	3.7	Hill et al. (1969)	
17 Jan. 1967	117	0.072	3.7	Hill et al. (1969)	
11 Mar. 1967	142	0.068	3.5	Hill and Hinteregger (1970)	
22 Mar. 1967	150	0.074	3.8	Fall et al. (1969)	
15 May 1967	111	0.056	2.9	Hill and Hinteregger (1970)	
24 May 1967	201	0.079	4.1	Hill and Hinteregger (1970)	
15 Aug. 1967	127	0.066	3.5	Hill et al. (1969)	
30 Sep. 1967	132	0.058	3.0	Hill et al. (1969)	
19 Feb. 1968	138	0.072	3.7	Hill et al. (1969)	
21 Feb. 1968	134	0.072	3.7	Hill et al. (1969)	

Table A-3.3
Intensity Measurements of the C VI Line at 33.7A°

Date	10.7 cm Flux	Intensity of 33.7A° Line		Reference
	($10^{-22} \text{ Wm}^{-2} \text{ Hz}^{-1}$)	(ergs $\text{cm}^{-2} \text{ sec}^{-1}$)		
20 Sep. 1963	109	0.062		Austin et al. (1966);
5 Aug. 1964	71	0.019		Argo et al. (1970)
3 Nov. 1965	80	0.004		Manson (1967, 1968)
3 Aug. 1966	98	0.029		Argo et al. (1970)
11 Aug. 1966	93	0.022		Argo et al. (1970)
12 Nov. 1966	126	0.014		Argo et al. (1970)
8 Aug. 1967	143	0.002		Hinteregger (1970)
3 Oct. 1967	132	0.066		Argo et al. (1970)
20 Mar. 1968	130	0.009		Freeman and Jones (1970)
20 Nov. 1969	189	0.007		Freeman and Jones (1970)

PRECEDING PAGE BLANK NOT FILMED

APPENDIX A-4

Number of Molecule : Along Line of Sight

In Tables A-4 we list for several solar zenith angles the number of O, O₂, and N₂ molecules along the line of sight to the sun (i.e. $S(z, \chi)$ of section 5.2). To calculate this quantity we assume our model atmosphere to be spherically symmetric. At an altitude z we construct 50 concentric shells, each of thickness $\tau = 1$ km. From the geometry of Fig. A-4 we have

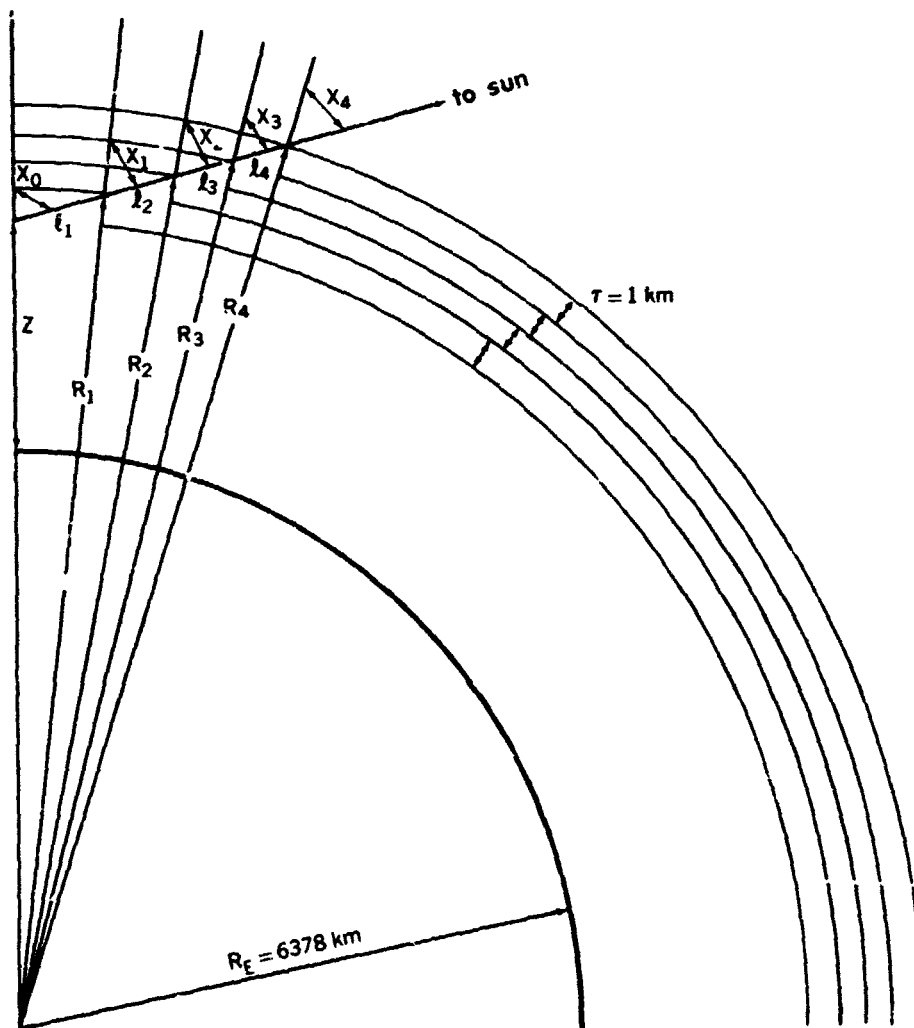


Figure A-4. Geometry for calculating $S(z, \chi)$, the number of molecules along the line of sight to the sun.

$$R_3^2 = R_2^2 + \ell_3^2 - 2R_2\ell_3 \cos(\pi - \chi_2) \quad (1)$$

$$R_n^2 = R_{n-1}^2 + \ell_n^2 - 2R_{n-1}\ell_n \cos(\pi - \chi_{n-1}) \quad (2)$$

$$\ell_n^2 - 2[R_{n-1} \cos(\pi - \chi_{n-1})] \ell_n - (R_n^2 - R_{n-1}^2) = 0 \quad (3)$$

$$\ell_n = R_{n-1} \cos(\pi - \chi_{n-1}) + \sqrt{[R_{n-1} \cos(\pi - \chi_{n-1})]^2 + (R_n^2 - R_{n-1}^2)} \quad (4)$$

$$\frac{\sin \chi_3}{R_2} = \frac{\sin(\pi - \chi_2)}{R_3} = \frac{\sin \chi_2}{R_3} \quad (5)$$

$$\frac{\sin \chi_n}{R_{n-1}} = \frac{\sin \chi_{n-1}}{R_n} \quad (6)$$

$$\sin \chi_n = \left(\frac{R_{n-1}}{R_n} \right) \sin \chi_{n-1} \quad (7)$$

$$R_n = R_0 + n \quad (8)$$

$$R_0 = R_E + Z \quad (9)$$

$$R_E = 6378.0 \text{ (radius of Earth at equator)} \quad (10)$$

$$S(z, \chi_0) = \sum_{n=1}^{50} \ell_n \left(\frac{\rho_y + \rho_{y+1}}{2} \right) \quad (11)$$

where

$$\left(\frac{\rho_y + \rho_{y+1}}{2} \right)$$

is average density in nth shell

$$y = Z + n - 1 \quad (12)$$

Table A-4.1

Alt	$\chi = 10^\circ$			$\chi = 40^\circ$		
	S_{O_2}	S_{O_2}	S_{N_2}	S_{O_2}	S_{O_2}	S_{N_2}
6.00E1	2.18E18	1.13E21	4.23E21	2.79E18	1.46E21	5.44E21
6.10E1	2.22E18	1.13E21	4.23E21	2.85E18	1.27E21	4.74E21
6.20E1	2.26E18	8.60E20	3.21E21	2.90E18	1.10E21	4.12E21
6.30E1	2.30E18	7.47E20	2.79E21	2.94E18	9.59E20	3.58E21
6.40E1	2.33E18	6.47E20	2.42E21	2.98E18	8.31E20	3.10E21
6.50E1	2.35E18	5.59E20	2.09E21	3.02E18	7.18E20	2.68E21
6.60E1	2.38E18	4.82E20	1.80E21	3.04E18	6.19E20	2.32E21
6.70E1	2.40E18	4.15E20	1.55E21	3.08E18	5.33E20	1.99E21
6.80E1	2.42E18	3.56E20	1.33E21	3.11E18	4.58E20	1.71E21
6.90E1	2.44E18	3.05E20	1.14E21	3.13E18	3.92E20	1.47E21
7.00E1	2.46E18	2.60E20	9.75E20	3.16E18	3.34E20	1.25E21
7.10E1	2.48E18	2.21E20	8.31E20	3.18E18	2.85E20	1.07E21
7.20E1	2.49E18	1.88E20	7.07E20	3.20E18	2.42E20	9.09E20
7.30E1	2.51E18	1.60E20	6.01E20	3.21E18	2.05E20	7.73E20
7.40E1	2.52E18	1.36E20	5.11E20	3.23E18	1.74E20	6.56E20
7.50E1	2.53E18	1.15E20	4.33E20	3.25E18	1.47E20	5.56E20
7.60E1	2.54E18	9.70E19	3.67E20	3.26E18	1.25E20	4.71E20
7.70E1	2.55E18	8.19E19	3.10E20	3.27E18	1.05E20	3.99E20
7.80E1	2.56E18	6.91E19	2.63E20	3.29E18	8.88E19	3.38E20
7.90E1	2.57E18	5.83E19	2.23E20	3.30E18	7.49E19	2.86E20
8.00E1	2.58E18	4.92E19	1.88E20	3.31E18	6.32E19	2.42E20
8.10E1	2.59E18	4.14E19	1.60E20	3.32E18	5.32E19	2.05E20
8.20E1	2.59E18	3.48E19	1.35E20	3.33E18	4.48E19	1.74E20
8.30E1	2.60E18	2.93E19	1.14E20	3.34E18	3.76E19	1.47E20
8.40E1	2.61E18	2.46E19	9.70E19	3.35E18	3.16E19	1.25E20
8.50E1	2.61E18	2.06E19	8.22E19	3.35E18	2.65E19	1.06E20
8.60E1	2.62E18	1.73E19	6.97E19	3.36E18	2.22E19	8.95E19
8.70E1	2.62E18	1.44E19	5.90E19	3.37E18	1.85E19	7.58E19
8.80E1	2.63E18	1.20E19	4.99E19	3.38E18	1.55E19	6.41E19
8.90E1	2.64E18	9.98E18	4.22E19	3.38E18	1.28E19	5.42E19
9.00E1	2.60E18	8.25E18	3.56E19	3.34E18	1.06E19	4.57E19
9.10E1	2.52E18	6.80E18	3.00E19	3.23E18	8.74E18	3.86E19
9.20E1	2.42E18	5.60E18	2.53E19	3.11E18	7.19E18	3.25E19
9.30E1	2.31E18	4.61E18	2.13E19	2.97E18	5.92E18	2.74E19
9.40E1	2.18E18	3.78E18	1.79E19	2.80E18	4.86E18	2.30E19
9.50E1	2.02E18	3.11E18	1.51E19	2.60E18	3.99E18	1.94E19
9.60E1	1.86E18	2.55E18	1.27E19	2.39E18	3.27E18	1.63E19
9.70E1	1.70E18	2.09E18	1.07E19	2.19E18	2.69E18	1.37E19
9.80E1	1.56E18	1.72E18	9.01E18	2.00E18	2.22E18	1.16E19
9.90E1	1.42E18	1.42E18	7.62E18	1.82E18	1.83E18	9.79E18
1.00E2	1.29E18	1.18E18	6.45E18	1.65E18	1.51E18	8.29E18
1.01E2	1.17E18	9.78E17	5.48E18	1.50E18	1.26E18	7.04E18
1.02E2	1.06E18	8.14E17	4.66E18	1.36E18	1.05E18	5.99E18
1.03E2	9.63E17	6.80E17	3.98E18	1.24E18	8.73E17	5.11E18
1.04E2	8.76E17	5.70E17	3.41E18	1.13E18	7.32E17	4.38E18
1.05E2	7.99E17	4.80E17	2.93E18	1.03E18	6.16E17	3.76E18
1.06E2	7.30E17	4.05E17	2.52E18	9.37E17	5.21E17	3.24E18
1.07E2	6.68E17	3.44E17	2.18E18	8.58E17	4.41E17	2.80E18
1.08E2	6.13E17	2.93E17	1.90E18	7.87E17	3.76E17	2.43E18
1.09E2	5.63E17	2.50E17	1.65E18	7.23E17	3.21E17	2.12E18
1.10E2	5.18E17	2.15E17	1.45E18	6.66E17	2.76E17	1.86E18

Table A-4.2

Alt	$\chi = 60^\circ$			$\chi = 75^\circ$		
	S_O	S_{O_2}	S_{N_2}	S_O	S_{O_2}	S_{N_2}
6.00E1	4.22E18	2.23E21	8.31E21	7.69E18	4.25E21	1.59E22
6.10E1	4.31E18	1.94E21	7.24E21	7.85E18	3.71E21	1.38E22
6.20E1	4.38E18	1.69E21	6.30E21	8.00E18	3.23E21	1.20E22
6.30E1	4.45E18	1.47E21	5.48E21	8.13E18	2.80E21	1.05E22
6.40E1	4.51E18	1.27E21	4.75E21	8.25E18	2.43E21	9.07E21
6.50E1	4.57E18	1.10E21	4.10E21	8.37E18	2.10E21	7.84E21
6.60E1	4.62E18	9.47E20	3.54E21	8.47E18	1.81E21	6.77E21
6.70E1	4.66E18	8.15E20	3.05E21	8.57E18	1.56E21	5.83E21
6.80E1	4.71E18	7.00E20	2.62E21	8.66E18	1.34E21	5.01E21
6.90E1	4.75E18	5.99E20	2.24E21	8.74E18	1.15E21	4.29E21
7.00E1	4.78E18	5.11E20	1.91E21	8.82E18	9.78E20	3.66E21
7.10E1	4.82E18	4.35E20	1.63E21	8.89E18	8.32E20	3.12E21
7.20E1	4.85E18	3.70E20	1.39E21	8.96E18	7.08E20	2.66E21
7.30E1	4.98E18	3.14E20	1.18E21	9.02E18	6.01E20	2.26E21
7.40E1	4.90E18	2.66E20	1.00E21	9.09E18	5.10E20	1.92E21
7.50E1	4.93E18	2.25E20	8.50E20	9.14E18	4.31E20	1.63E21
7.60E1	4.95E18	1.90E20	7.20E20	9.20E18	3.65E20	1.38E21
7.70E1	4.97E18	1.61E20	6.10E20	9.25E18	3.08E20	1.17E21
7.80E1	4.99E18	1.36E20	5.16E20	9.30E18	2.60E20	9.88E20
7.90E1	5.01E18	1.15E20	4.37E20	9.35E18	2.19E20	8.37E20
8.00E1	5.03E18	9.66E19	3.70E20	9.40E18	1.85E20	7.08E20
8.10E1	5.05E18	8.13E19	3.13E20	9.44E18	1.56E20	6.00E20
8.20E1	5.06E18	6.84E19	2.65E20	9.49E18	1.31E20	5.08E20
8.30E1	5.08E18	5.76E19	2.25E20	9.53E18	1.07E20	4.30E20
8.40E1	5.10E18	4.83E19	1.90E20	9.57E18	9.26E19	3.64E20
8.50E1	5.11E18	4.05E19	1.61E20	9.61E18	7.77E19	3.09E20
8.60E1	5.12E18	3.40E19	1.37E20	9.65E18	6.50E19	2.62E20
8.70E1	5.14E18	2.84E19	1.16E20	9.69E18	5.43E19	2.22E20
8.80E1	5.15E18	2.36E19	9.81E19	9.73E18	4.53E19	1.88E20
8.90E1	5.16E18	1.96E19	8.29E19	9.76E18	3.76E19	1.59E20
9.00E1	5.09E18	1.62E19	6.99E19	9.65E18	3.11E19	1.34E20
9.10E1	4.93E18	1.34E19	5.90E19	9.36E18	2.56E19	1.13E20
9.20E1	4.75E18	1.10E19	4.97E19	9.01E18	2.11E19	9.51E19
9.30E1	4.53E18	9.05E18	4.19E19	8.60E18	1.73E19	8.01E19
9.40E1	4.27E18	7.44E18	3.52E19	8.11E18	1.42E19	6.74E19
9.50E1	3.96E18	6.10E18	2.96E19	7.53E18	1.17E19	5.67E19
9.60E1	3.64E18	5.01E18	2.49E19	6.92E18	9.58E18	4.76E19
9.70E1	3.34E18	4.11E18	2.10E19	6.34E18	7.87E18	4.01E19
9.80E1	3.05E18	3.39E18	1.77E19	5.80E18	6.48E18	3.38E19
9.90E1	2.78E18	2.80E18	1.50E19	5.28E18	5.35E18	2.86E19
1.00E2	2.52E18	2.31E18	1.27E19	4.79E18	4.43E18	2.42E19
1.01E2	2.29E18	1.92E18	1.08E19	4.34E18	3.67E18	2.06E19
1.02E2	2.08E18	1.60E18	9.16E18	3.94E18	3.06E18	1.75E19
1.03E2	1.89E18	1.33E18	7.81E18	3.58E18	2.55E18	1.49E19
1.04E2	1.72E18	1.12E18	6.69E18	3.26E18	2.14E18	1.28E19
1.05E2	1.57E18	9.42E17	5.75E18	2.97E18	1.80E18	1.10E19
1.06E2	1.43E18	7.96E17	4.95E18	2.71E18	1.52E18	9.45E18
1.07E2	1.31E18	6.75E17	4.28E18	2.48E18	1.29E18	8.17E18
1.08E2	1.20E18	5.74E17	3.72E18	2.27E18	1.10E18	7.09E18
1.09E2	1.10E18	4.91E17	3.24E18	2.09E18	9.37E17	6.17E18
1.10E2	1.02E18	4.22E17	2.83E18	1.92E18	8.05E17	5.40E18

APPENDIX A-5

Q-Function Components and r.m.s Error

Calculated values of the total Q-function together with the important components are listed in tables A-5 for several values of solar zenith angle. The final column labeled $\Delta Q/Q$ is our estimate of the relative error on $Q(z, \chi)$. To obtain this estimate we consider each component q_i to have an independent relative error given by

$$\left(\frac{\partial q_i}{q_i}\right)^2 \simeq \left(\frac{\partial F_i}{F_i}\right)^2 + \left(\frac{\partial N_j}{N_j}\right)^2 + \left(\frac{\partial \gamma_{ij}}{\gamma_{ij}}\right)^2 + (1 + \sigma_{ij} S_j)^2 \left(\frac{\partial \sigma_{ij}}{\sigma_{ij}}\right)^2$$

To evaluate this expression we assume somewhat arbitrarily the following uncertainties,

flux	$\partial F_i / F_i = .25$
cross section	$\partial \sigma_{ij} / \sigma_{ij} = \frac{\partial \gamma_{ij}}{\gamma_{ij}} = .10$
atmospheric density	$\partial N_j / N_j = .20$
nitric oxide	$\partial NO / NO = 1.0$

For the following components of Q we have used the uncertainties

q(1025-991A)	$\partial q / q = 1.0$
q(977A)	$\partial q / q = 1.0$
q(O ₂ [*])	$\partial q / q = 2.0$
q(background)	$\partial q / q = 1.0$

The relative error on Q is then obtained from

$$\left(\frac{\Delta Q}{Q}\right)^2 = \sum_i \left(q_i \times \left(\frac{\partial q_i}{q_i}\right) \right)^2$$

TABLE A-5.1

ALP	LYNAR ALPHA	LYNAR RPPA	PWY 1025-9900	CITZ 877A	X-RAY 103-01A	X-RAY 81-33A	X-RAY 51-10A	X-RAY 10-1A	MPRSTB CXTOP	BACK GROUND	TOTAL C	ERROR AK/C
60	8.39F03									8.39F03	1.34E02	0.91
61	1.61F02									7.81E01	2.37E02	1.11
62	4.81F02									8.29E01	1.20E01	1.41
63	1.23F01									6.28E01	2.56E01	1.46
64	2.50F01									6.11E01	4.94E01	1.40
65	8.87F01									7.81E02	7.77E01	1.36
66	8.84F01									1.04E02	3.48E00	1.33
67	1.47F00									1.82E02	2.13E00	1.30
68	2.11F00									1.97E02	2.99E00	1.27
69	2.47F00									2.71E02	4.92E00	1.24
70	3.96F00									3.53E02	4.94E00	1.21
71	4.86F00									4.48E02	6.66E00	1.19
72	5.78F00									5.42E02	8.68E00	1.17
73	6.43F00									6.38E02	7.77E00	1.15
74	7.16F00									7.38E02	8.06E00	1.13
75	7.80F00									8.32E02	8.33E00	1.11
76	7.82F00									9.22E02	8.36E00	1.09
77	7.83F00									1.01E03	8.39E00	1.07
78	7.73F00									1.10E03	8.29E00	1.05
79	7.60F00									1.20E03	8.23E00	1.03
80	7.34F00									1.33E03	8.13E00	1.01
81	7.18F00									1.47E03	8.03E00	0.99
82	6.98F00									1.62E03	8.00E00	0.97
83	6.85F00									1.78E03	8.00E00	0.94
84	6.85F00									1.94E03	8.00E00	0.91
85	7.16F00									2.10E03	8.00E00	0.89
86	7.71F00									2.27E03	8.00E00	0.87
87	8.70F00									2.45E03	8.00E00	0.85
88	1.03F01	7.58F01	4.80F01	1.84F01	1.00F01	1.00F01	1.00F01	1.00F01		2.64E03	8.00E01	0.83
89	1.42F01	1.45F01	3.02F01	1.06F01	1.06F01	1.06F01	1.06F01	1.06F01		2.84E03	8.00E01	0.81
90	1.82F01	1.72F01	4.24F01	1.34F01	1.34F01	1.34F01	1.34F01	1.34F01		3.05E03	8.00E01	0.79
91	2.06F01	1.90F01	5.47F01	1.63F01	1.63F01	1.63F01	1.63F01	1.63F01		3.27E03	8.00E01	0.77
92	2.31F01	2.08F01	6.70F01	1.93F01	1.93F01	1.93F01	1.93F01	1.93F01		3.50E03	8.00E01	0.75
93	2.56F01	2.28F01	8.03F01	2.24F01	2.24F01	2.24F01	2.24F01	2.24F01		3.74E03	8.00E01	0.73
94	3.03F01	2.55F01	9.46F01	2.56F01	2.56F01	2.56F01	2.56F01	2.56F01		4.00E03	8.00E01	0.71
95	3.40F01	3.02F01	1.09F02	2.88F01	2.88F01	2.88F01	2.88F01	2.88F01		4.27E03	8.00E01	0.69
96	3.79F01	3.22F01	1.42F02	3.21F01	3.21F01	3.21F01	3.21F01	3.21F01		4.55E03	8.00E01	0.67
97	4.22F01	3.42F01	1.75F02	3.54F01	3.54F01	3.54F01	3.54F01	3.54F01		4.84E03	8.00E01	0.65
98	4.67F01	3.63F01	2.08F02	3.88F01	3.88F01	3.88F01	3.88F01	3.88F01		5.14E03	8.00E01	0.63
99	5.13F01	3.85F01	2.41F02	4.23F01	4.23F01	4.23F01	4.23F01	4.23F01		5.45E03	8.00E01	0.61
100	5.61F01	4.08F01	2.74F02	4.58F01	4.58F01	4.58F01	4.58F01	4.58F01		5.77E03	8.00E01	0.59
101	6.09F01	4.32F01	3.07F02	4.94F01	4.94F01	4.94F01	4.94F01	4.94F01		6.10E03	8.00E01	0.57
102	6.57F01	4.57F01	3.40F02	5.30F01	5.30F01	5.30F01	5.30F01	5.30F01		6.44E03	8.00E01	0.55
103	7.06F01	4.82F01	3.73F02	5.66F01	5.66F01	5.66F01	5.66F01	5.66F01		6.79E03	8.00E01	0.53
104	7.56F01	5.07F01	4.06F02	6.02F01	6.02F01	6.02F01	6.02F01	6.02F01		7.14E03	8.00E01	0.51
105	8.06F01	5.32F01	4.40F02	6.38F01	6.38F01	6.38F01	6.38F01	6.38F01		7.50E03	8.00E01	0.49
106	8.57F01	5.57F01	4.74F02	6.74F01	6.74F01	6.74F01	6.74F01	6.74F01		7.87E03	8.00E01	0.47
107	9.08F01	5.82F01	5.08F02	7.10F01	7.10F01	7.10F01	7.10F01	7.10F01		8.24E03	8.00E01	0.45
108	9.59F01	6.07F01	5.42F02	7.46F01	7.46F01	7.46F01	7.46F01	7.46F01		8.62E03	8.00E01	0.43
109	10.10F01	6.32F01	5.76F02	7.82F01	7.82F01	7.82F01	7.82F01	7.82F01		9.00E03	8.00E01	0.41
110	10.61F01	6.57F01	6.10F02	8.18F01	8.18F01	8.18F01	8.18F01	8.18F01		9.38E03	8.00E01	0.39

X = 10⁰

* BACKGROUND: I.P. SCATTERED LYNAR-ALPHA, SCATTERED LYNAR-BETA AND COSMIC RAYS

TABLE A-5.2

ALT	LYMAN ALPHA	LYMAN BETA	FUV 1025-590Å	GIII 977Å	K-RAY 103-41Å	K-RAY 41-31Å	K-RAY 31-10Å	X-RAY 10-1Å	NEUTRONS OXYGEN	+RACK GROUP	TOTAL σ	ERROR $\Delta\sigma/\sigma$
60	1.20E ⁻⁰³									9.59E ⁻⁰³	8.59E ⁻⁰³	1.00
61	4.82E ⁻⁰³									7.61E ⁻⁰³	8.81E ⁻⁰³	0.91
62	1.59E ⁻⁰²									6.81E ⁻⁰³	1.16E ⁻⁰²	0.98
63	4.56E ⁻⁰²									6.26E ⁻⁰³	2.22E ⁻⁰²	1.31
64	1.12E ⁻⁰¹									6.11E ⁻⁰³	5.17E ⁻⁰²	1.50
65	2.44E ⁻⁰¹									7.81E ⁻⁰²	1.19E ⁻⁰¹	1.54
66	4.93E ⁻⁰¹									1.06E ⁻⁰²	5.04E ⁻⁰¹	1.48
67	8.29E ⁻⁰¹									1.42E ⁻⁰²	8.44E ⁻⁰¹	1.44
68	1.33E ⁰⁰									1.97E ⁻⁰²	1.35E ⁰⁰	1.44
69	2.00E ⁰⁰									2.71E ⁻⁰²	2.03E ⁰⁰	1.38
70	2.72E ⁰⁰									3.53E ⁻⁰²	2.76E ⁰⁰	1.15
71	3.51E ⁰⁰									4.45E ⁻⁰²	3.57E ⁰⁰	1.33
72	4.29E ⁰⁰									5.42E ⁻⁰¹	4.37E ⁰⁰	1.31
73	5.02E ⁰⁰									6.36E ⁻⁰¹	5.13E ⁰⁰	1.23
74	5.55E ⁰⁰									7.18E ⁻⁰¹	5.71E ⁰⁰	1.22
75	5.96E ⁰⁰									7.88E ⁻⁰¹	6.18E ⁰⁰	1.24
76	6.32E ⁰⁰									8.58E ⁻⁰¹	6.83E ⁰⁰	1.22
77	6.64E ⁰⁰									9.22E ⁻⁰¹	7.45E ⁰⁰	1.20
78	6.92E ⁰⁰									9.82E ⁻⁰¹	7.94E ⁰⁰	1.19
79	7.17E ⁰⁰									1.04E ⁻⁰¹	8.48E ⁰⁰	1.19
80	7.39E ⁰⁰									1.10E ⁻⁰¹	9.02E ⁰⁰	1.19
81	7.58E ⁰⁰									1.16E ⁻⁰¹	9.57E ⁰⁰	1.13
82	7.74E ⁰⁰									1.22E ⁻⁰¹	1.01E ⁰¹	1.10
83	7.87E ⁰⁰									1.28E ⁻⁰¹	1.06E ⁰¹	1.07
84	7.97E ⁰⁰									1.34E ⁻⁰¹	1.11E ⁰¹	1.05
85	8.05E ⁰⁰									1.40E ⁻⁰¹	1.16E ⁰¹	1.03
86	8.11E ⁰⁰									1.46E ⁻⁰¹	1.21E ⁰¹	1.02
87	8.16E ⁰⁰									1.52E ⁻⁰¹	1.26E ⁰¹	1.00
88	8.20E ⁰⁰									1.58E ⁻⁰¹	1.31E ⁰¹	0.98
89	8.23E ⁰⁰									1.64E ⁻⁰¹	1.36E ⁰¹	0.96
90	8.25E ⁰⁰									1.70E ⁻⁰¹	1.41E ⁰¹	0.93
91	8.26E ⁰⁰									1.76E ⁻⁰¹	1.46E ⁰¹	0.91
92	8.26E ⁰⁰									1.82E ⁻⁰¹	1.51E ⁰¹	0.89
93	8.25E ⁰⁰									1.88E ⁻⁰¹	1.56E ⁰¹	0.87
94	8.23E ⁰⁰									1.94E ⁻⁰¹	1.61E ⁰¹	0.85
95	8.19E ⁰⁰									2.00E ⁻⁰¹	1.66E ⁰¹	0.83
96	8.14E ⁰⁰									2.06E ⁻⁰¹	1.71E ⁰¹	0.81
97	8.08E ⁰⁰									2.12E ⁻⁰¹	1.76E ⁰¹	0.79
98	8.01E ⁰⁰									2.18E ⁻⁰¹	1.81E ⁰¹	0.77
99	7.93E ⁰⁰									2.24E ⁻⁰¹	1.86E ⁰¹	0.75
100	7.84E ⁰⁰									2.30E ⁻⁰¹	1.91E ⁰¹	0.73
101	7.74E ⁰⁰									2.36E ⁻⁰¹	1.96E ⁰¹	0.71
102	7.63E ⁰⁰									2.42E ⁻⁰¹	2.01E ⁰¹	0.69
103	7.51E ⁰⁰									2.48E ⁻⁰¹	2.06E ⁰¹	0.67
104	7.38E ⁰⁰									2.54E ⁻⁰¹	2.11E ⁰¹	0.65
105	7.24E ⁰⁰									2.60E ⁻⁰¹	2.16E ⁰¹	0.63
106	7.09E ⁰⁰									2.66E ⁻⁰¹	2.21E ⁰¹	0.61
107	6.93E ⁰⁰									2.72E ⁻⁰¹	2.26E ⁰¹	0.59
108	6.76E ⁰⁰									2.78E ⁻⁰¹	2.31E ⁰¹	0.57
109	6.58E ⁰⁰									2.84E ⁻⁰¹	2.36E ⁰¹	0.55
110	6.39E ⁰⁰									2.90E ⁻⁰¹	2.41E ⁰¹	0.53

X = 40°

+ RACKGROUP: I.K. SCATTERED LYMAN-ALPHA, SCATTERED LYMAN-BETA AND COSMIC RAYS

TABLE A-5.3

ALT	LYMAN ALPHA	LYMAN BETA	EDF 1025-9904	CIII 977A	X-RAY 103-41A	X-RAY 41-31A	X-RAY 31-10A	X-RAY 10-1A	METASTB DTYGER	*RACY GROUND	TOTAL Q	ERROR AQ/R
60										8.59E-03	9.59E-03	1.00
61										7.61E-03	7.61E-03	1.00
62										6.81E-03	6.81E-03	1.00
63										6.26E-03	6.26E-03	1.00
64	7.92E-04									6.11E-03	6.90E-03	0.93
65	3.38E-03									6.54E-03	9.92E-02	0.96
66	1.19E-02									7.61E-02	1.97E-02	1.19
67	3.67E-02									1.06E-02	4.79E-02	1.42
68	8.90E-02									1.42E-02	1.03E-01	1.55
69	1.97E-01									1.97E-02	2.17E-01	1.81
70	3.91E-01									2.71E-02	4.18E-01	1.63
71	6.78E-01									3.53E-02	7.14E-01	1.63
72	1.08E+00								4.79E-04	4.45E-02	1.12E+00	1.62
73	1.57E+00									5.42E-01	1.63E+00	1.60
74	2.14E+00							5.98E-04	4.28E-03	6.38E-01	2.21E+00	1.58
75	2.70E+00							1.12E-03	1.25E-02	7.18E-01	2.79E+00	1.57
76	3.24E+00							2.06E-03	2.75E-02	7.88E-01	3.35E+00	1.55
77	3.78E+00							3.70E-03	5.25E-02	8.58E-01	3.92E+00	1.53
78	4.18E+00							4.49E-03	8.99E-02	9.02E-01	4.38E+00	1.50
79	4.52E+00							1.10E-02	1.41E-01	9.42E-01	4.77E+00	1.48
80	4.74E+00							1.83E-02	2.04E-01	9.62E-01	5.05E+00	1.46
81	4.97E+00							2.57E-02	2.75E-01	9.93E-01	5.37E+00	1.43
82	5.12E+00							4.69E-02	3.49E-01	1.01E-01	5.61E+00	1.41
83	5.28E+00							7.26E-02	4.18E-01	1.04E-01	5.87E+00	1.38
84	5.50E+00							1.10E-01	4.60E-01	1.08E-01	6.20E+00	1.36
85	5.95E+00							1.64E-01	5.31E-01	1.18E-01	6.72E+00	1.35
86	6.61E+00							2.40E-01	5.70E-01	1.31E-01	7.58E+00	1.34
87	7.65E+00							3.49E-01	5.86E-01	1.53E-01	8.74E+00	1.34
88	9.28E+00							4.88E-01	5.91E-01	1.87E-01	1.08E+01	1.34
89	1.20E+01							6.76E-01	5.78E-01	2.23E-01	1.38E+01	1.35
90	1.56E+01							9.30E-01	5.58E-01	3.23E-01	1.76E+01	1.33
91	1.88E+01							1.24E+00	5.34E-01	3.97E-01	2.13E+01	1.27
92	2.21E+01							1.60E+00	4.06E-01	4.87E-01	2.62E+01	1.17
93	2.55E+01							2.05E+00	4.34E-01	6.21E-01	3.22E+01	1.04
94	2.93E+01							2.53E+00	4.04E-01	8.78E-01	4.07E+01	0.90
95	3.30E+01							3.03E+00	3.59E-01	1.35E+00	5.33E+01	0.74
96	3.70E+01							3.49E+00	3.16E-01	2.19E+00	7.45E+01	0.59
97	4.14E+01							3.85E+00	2.78E-01	3.46E+00	1.12E+02	0.46
98	4.60E+01							4.10E+00	2.43E-01	5.15E+01	1.77E+02	0.36
99	5.08E+01							4.23E+00	2.07E-01	7.13E+01	2.78E+02	0.31
100	5.65E+01							4.24E+00	1.77E-01	9.22E+01	4.21E+02	0.28
101	5.99E+01							4.15E+00	1.53E-01	1.12E+01	5.99E+02	0.27
102	6.34E+01							3.98E+00	1.32E-01	1.29E+01	8.00E+02	0.27
103	6.95E+01							3.73E+00	1.16E-01	1.42E+01	1.01E+03	0.27
104	7.42E+01							3.43E+00	1.02E-01	1.50E+01	1.22E+03	0.27
105	7.12E+01							3.14E+00	8.75E-02	1.53E+01	1.41E+03	0.28
106	7.32E+01							2.89E+00	7.54E-02	1.53E+01	1.59E+03	0.29
107	7.52E+01							2.66E+00	6.39E-02	1.50E+01	1.74E+03	0.30
108	7.53E+01							2.29E+00	5.41E-02	1.44E+01	1.85E+03	0.32
109	7.22E+01							2.03E+00	4.91E-02	1.36E+01	1.92E+03	0.34
110	7.03E+01							1.79E+00	4.46E-02	1.26E+01	1.94E+03	0.35

$\chi = 60^\circ$

..... I.F. SCATTERED LYMAN-ALPHA, SCATTERED LYMAN-BETA AND COSMIC RAYS

TABLE A-5.4

ALT	LIMAN ALPHA	LIMAN BETA	FUV 1025-990A	CIIT 977A	X-RAY 103-41A	X-RAY 41-31A	X-RAY 31-10A	X-RAY 10-1A	NETASTB CYCLEN	+BACK GROUND	TOTAL C	ERROR ΔC/C
60										8.59E-03	8.59E-03	1.00
61										7.61E-03	7.61E-03	1.00
62										6.81E-03	6.81E-03	1.00
63										6.26E-03	6.26E-03	1.00
64										6.11E-03	6.11E-03	1.00
65										6.54E-03	6.54E-03	1.00
66										7.81E-02	7.81E-02	1.00
67										1.06E-02	1.06E-02	1.00
68										1.42E-02	1.42E-02	1.00
69	1.27E-03									1.97E-02	2.10E-02	0.97
70	5.28E-03									2.71E-02	3.24E-02	0.95
71	1.74E-02									3.53E-02	5.28E-02	1.00
72	4.77E-02									4.95E-02	9.23E-01	1.21
73	1.11E-01									5.82E-01	1.66E-01	1.52
74	2.27E-01									6.38E-01	2.91E-01	1.60
75	4.04E-01									7.88E-01	4.76E-01	2.01
76	6.51E-01									8.58E-01	7.30E-01	2.15
77	9.73E-01									9.02E-01	1.06E00	2.23
78	1.33E00									9.02E-01	1.42E00	2.28
79	1.72E00									9.42E-01	1.83E00	2.30
80	2.10E00									9.82E-01	2.22E00	2.31
81	2.50E00									9.93E-01	2.65E00	2.31
82	2.87E00									1.01E-01	3.05E00	2.30
83	3.23E00									1.04E-01	3.47E00	2.28
84	3.68E00									1.08E-01	3.94E00	2.26
85	4.23E00									1.18E-01	4.58E00	2.25
86	4.96E00									1.31E-01	5.39E00	2.25
87	5.82E00									1.53E-01	6.52E00	2.25
88	7.00E00									1.87E-01	8.20E00	2.27
89	1.02E01									2.45E-01	1.09E01	2.20
90	1.36E01									3.28E-01	1.45E01	2.28
91	1.68E01									3.97E-01	1.78E01	2.22
92	2.02E01									4.87E-01	2.13E01	2.15
93	2.37E01									6.21E00	2.51E01	2.06
94	2.75E01									8.79E00	2.94E01	1.70
95	3.14E01									1.13E01	3.41E01	1.70
96	3.55E01									1.49E01	3.98E01	1.50
97	3.99E01									1.98E01	4.70E01	1.37
98	4.47E01									2.59E01	5.62E01	1.10
99	4.94E01									3.35E01	6.84E01	1.00
100	5.48E01									4.28E01	8.47E01	0.84
101	6.09E01									5.42E01	1.04E02	0.68
102	6.73E01									6.79E01	1.24E02	0.54
103	7.41E01									8.38E01	1.49E02	0.43
104	8.13E01									1.03E02	1.79E02	0.36
105	8.89E01									1.28E02	2.10E02	0.32
106	9.69E01									1.58E02	2.45E02	0.30
107	1.05E02									1.94E02	2.85E02	0.29
108	1.14E02									2.35E02	3.30E02	0.28
109	1.24E02									2.82E02	3.84E02	0.28
110	1.35E02									3.35E02	4.44E02	0.28
111	1.47E02									3.94E02	5.11E02	0.29

X = 75°

* BACKGROUND; I.F. SCATTERED LIMAN-ALPHA, SCATTERED LIMAN-BETA AND COSMIC RAYS

APPENDIX A-6

Equatorial Reference Electron Density Profile

In principal, the electron density distribution of the lower ionosphere from 60 km to 105 km can be accurately deduced from ground-based radio wave absorption and virtual height measurements, provided that the measurements are performed over a sufficiently wide range of frequencies, perhaps from about 0.25 MHz to 3.5 MHz. In practice, it has proved to be difficult to conduct experiments at frequencies less than 1.5 MHz partly because these frequencies fall within the broadcast band and also because the noon absorption is high at these frequencies, so that the reflected wave cannot be detected by conventional methods. The frequencies generally employed for D- and E-region absorption studies have therefore been limited to the range 1.6-3.5 MHz.

Electron density profiles have been derived from multi-frequency data acquired within this limited frequency range (Beynon and Rangaswamy, 1969); but there seems to be some uncertainty in the precise form of these profiles at altitudes below about 80 km. This is because the total absorption and its variation with frequency in the range 1.6-3.5 MHz is rather insensitive to the exact shape of the profile at these low altitudes. Here the absorption is entirely non-deviative and is a relatively small fraction of the total absorption.

Ground-based methods which yield more accurate profiles for altitudes below 80 km are the partial-reflection technique, wave-interaction experiments and propagation measurements at low- and very-low frequencies. But none of these methods has hitherto been exploited at equatorial latitudes. The few profiles that are available for these altitudes at the equator are those obtained from rocket-borne measurements at Thumba, India (Kane 1969, 1972, Somayajulu et al. 1971, Aikin et al. 1972).

In the present work we construct a reference electron density profile for a solar zenith angle $\chi = 10^\circ$, for the conditions of an undisturbed sun (1-8A flux less than 0.5×10^{-3} erg cm⁻² sec⁻¹) at solar cycle maximum, by combining the results of a noontime rocket measurement at Thumba, India with the results of multifrequency absorption and virtual height measurements made at Colombo, Ceylon. For the lowest segment of the profile from 60 km to 82 km we adopt the electron density distribution derived by Kane (1969) from rocket-borne absorption measurements obtained when the solar zenith angle was 14° . This is the smallest zenith angle for which rocket measurements are available. The electron density values computed by Kane have been corrected so as to be consistent with the current best estimates of collision frequency.

The uppermost portion of the profile depicts the E-layer maximum. The corresponding electron density is calculated from the critical frequency foE of the E-layer. Empirical formulas which give foE as a function of solar activity and zenith angle have been deduced from several decades of ionosonde data. The formulas used in the present work are listed below:

(a) Minnis (1964)

For noon foE,

$$(foE)^4 \sec \chi = 1.55 \Phi - 1.0 \times 10^{-3} \Phi^2 + 14$$

where

$$\Phi \text{ is the 10.7 cm flux in } 10^{-22} \text{ Wm}^{-2} \text{ Hz}^{-1}$$

(b) Lyon (1965)

Annual mean foE at Ibadan (07°22'N 03° 58'E) around noon is given by

$$\overline{foE} = 3.47(1 + 0.0014 R_z)$$

where R_z is the sunspot number. Since the noon foE varies with season in proportion to $\cos^{0.25} \chi$ this formula reduces to

$$foE = 3.52 \cos^{0.25} \chi (1 + 0.0014 R_z)$$

(c) Eyfrig and Rawer (1969)

$$foE = \left[3.44(1 - 0.1(1 - \cos\theta)) + \left\{ \frac{1}{200} (\Phi - 69) \right\}^{0.6} \right] \cos^{1/3} \chi$$

where θ is the geographic latitude and Φ is the 10.7 cm solar flux.

For the solar conditions appropriate to our reference profile, that is $\chi = 10^\circ$, $R_z = 85$ and $\Phi = 135$, the mean value of foE given by these formulas is 3.89 MHz corresponding to an electron density of $1.9 \times 10^5 \text{ cm}^{-3}$.

The altitude of the E-layer peak is calculated from the expression (Piggott and Thrane 1966)

$$h_m E = 105 + 7.5 \ln(\sec \chi) \text{ km.}$$

$$\text{For } \chi = 10^\circ, h_m E = 105.1 \approx 105 \text{ km.}$$

Noontime rocket-borne probe measurements conducted at equatorial latitudes (Aikin and Blumle 1968, Satya Prakash et al. 1971) have indicated that the E-region has a broad maximum of ionization which extends several kilometers above the peak altitude deduced from ionosonde records. For the reference profile we have therefore adopted a constant electron density of $1.9 \times 10^5 \text{ cm}^{-3}$ for the altitude range 105-110 km.

To determine the electron density distribution in the intervening region from 82 km to 105 km we first postulate an arbitrary distribution and then adjust it by trial and error until the calculated values of absorption and virtual height of vertically incident radiowaves of different frequencies are in good agreement with the ground-based measurements made at Colombo. The experimental data used for this purpose are those obtained with radio waves reflected from the E-layer, on the five frequencies 1.33, 2.0, 2.2, 2.6 and 3.2 MHz. The data on 1.33 MHz had been obtained by means of a special technique which enabled the detection of weak echoes (Gnanalingam 1954).

It is well known that the virtual height of reflection is particularly sensitive to the electron density gradient near the reflection level. So, our initial trials are directed towards finding a suitable profile for the bottomside of the E-layer. As a first step it is convenient to assume an electron density distribution that could be represented by one of the several formulas which have been postulated for the profiles of ionospheric layers (Budden 1961). The virtual height could then be readily computed from well-established analytical expressions. The profile selected by us as a first trial is the 'sech' profile given by the expression:-

$$N_e = 1.9 \times 10^5 \operatorname{sech}^2 \left(\frac{h - h_m}{H} \right)$$

where the symbols have their usual meaning. When the earth's magnetic field and electron collisions may be neglected the virtual height resulting from this profile is given by (Budden 1961, p. 157)

$$h'(f) = H \log \left[\left(\frac{f \sigma^2}{f^2} - 1 \right)^{-1/2} \sinh \frac{h_m}{H} + \left\{ \left(\frac{f \sigma^2}{f^2} - 1 \right)^{-1} \sinh^2 \frac{h_m}{H} - 1 \right\}^{1/2} \right]$$

This relation is also valid for an ordinary wave propagated vertically near the magnetic equator. For $H = 8 \text{ km}$, the virtual heights computed from this expression are listed together with the measured values:

Frequency (MHz):	1.33	2.0	2.2	2.6	3.2
True height h_c (km):	91.1	94.7	95.6	97.3	99.8
Computed h' (km):	96.8	100.8	101.9	104.1	107.8
Measured h' (km):	96.5	100.4	101.3	102.4	104.6

The discrepancies between the computed and measured virtual heights, particularly at the two higher frequencies, indicate that the electron densities have to be increased slightly at altitudes between 95 km and 105 km. The profile is modified accordingly. It is also found that the lower end of the 'sach²' profile has to be rounded off so that it merges smoothly with the Kane profile at 82 km.

We now have a composite profile from 60 km to 110 km. The absorption and virtual height resulting from this profile are next calculated by means of the generalized magnionic theory using the ray theory approximation. In calculating these quantities, the electron density and collision frequency values specified at 1 km intervals are logarithmically interpolated by the computer for altitude laminations of 100 meters. Since the complex refractive index changes vary rapidly immediately below the reflection level, the last 1 km of the ray trajectory is subdivided into smaller laminations of 10 meter thickness. The reflection level h_c is defined for the ordinary mode as the altitude at which the plasma frequency equals the frequency of the exploring radiowave.

To the absorption calculated by ray theory we add a phase integral correction which is computed from the approximate analytic expression derived by Thorpe (1971). Near the magnetic equator, this correction is relatively small. Thorpe has checked his results against the phase integral correction computed rigorously, and has found that his accuracy is better than 5-10% provided that the angle between the wave normal and the geomagnetic field is greater than 10° which, of course, is the case near the magnetic dip equator. At our exploring frequencies, this combination of a ray theory calculation plus a phase integral correction gives a good approximation to a full wave solution. We estimate that the overall accuracy of the absorption calculated by this method is better than ± 1.0 db.

To calculate the virtual height we note that, for an ordinary wave propagating vertically near the magnetic dip equator, the phase refractive index n and the group refractive index n' are related, to a good approximation, by the expression $nn' = 1$, provided that the effect of collisions may be neglected. Hence, from ray theory, the virtual height can be computed, with sufficient accuracy for our purpose, from the expression:

$$h' = \int_0^{h_c} \frac{1}{n(z)} dz$$

The advantage of using this expression is that n can be calculated more readily than n' . To the value of virtual height calculated by ray theory we must add a phase integral correction so as to give a result that is closely equivalent to a full-wave solution. Instead however, for ease of computation, we adopt an alternative procedure (Titheridge, 1967) in which $n(z)$ in the above integral is evaluated with the collision frequency set equal to zero. The accuracy of the virtual height resulting from this procedure is estimated to be better than ± 0.5 km.

The values of absorption and virtual height computed for the composite profile, for the five frequencies in the range 1.33-3.2 MHz, are now compared with the measurements. The profile in the altitude range 82-105 km is then suitably adjusted in the light of any discrepancies that are noted and the above procedure is repeated. This process of iteration is continued until there is good agreement between the calculated and measured quantities.

It is worth mentioning that the values of absorption and virtual height employed in the construction of the reference profile are the mean values of the noon measurements obtained on 72 days when the sun was undisturbed, that is 1-8Å solar X-ray flux less than 5×10^4 ergs $\text{cm}^{-2} \text{sec}^{-1}$, in the equinoctial months of 1968, 1969 and 1970 around solar cycle maximum. On 1.33 MHz, however, measurements were only available for 16 days.

The limits of uncertainty given in Table III for the measured absorption and virtual height need some comment. The figures for absorption, that is ± 6 db for 1.33 MHz and ± 2 db for 2.0, 2.2, 2.6 and 3.2 MHz, are estimates of the uncertainties in the calibration constants, and hence in the absolute magnitudes of the mean absorption. These estimates are based on the number of independent measurements that were obtained for the calibration constant on each frequency, and on the uncertainty (about ± 1 db) in the ground reflection coefficient.

The values of mean absorption are also subject to random errors arising partly from experimental errors and partly from the inherent variability of the ionosphere. The precision of the individual absorption measurements is estimated to be better than ± 2 db, and the standard deviation of the measurements in the 72-day sample is found to be about 2.5 db. Hence, the standard error of the mean absorption is approximately $\{(2^2 + 2.5^2)/71\}^{1/2} = 0.38$ db. This error is relatively small and is not therefore included in the table.

In the case of the virtual height measurements, the calibration accuracy of the measuring system is better than ± 0.1 km. Errors due to pulse rise-time effects are estimated to be less than 1 km. The principal source of uncertainty in the measurements is the distortion of the echo pulse caused by the 'roughness'

of the reflecting layer. This is a prominent feature of E-region echoes received near the magnetic dip equator and is a consequence of the irregularities associated with the electrojet. The leading edge of the echo pulse is ill-defined, so that the virtual height cannot be determined with great accuracy. The reading accuracy of each observation is no better than ± 2 km. The apparent variation in the virtual heights measured on the undisturbed days is probably due to this cause; and the standard deviation of these measurements may be regarded as indicative of the degree of roughness near the reflection level.

In Table III, the uncertainties in the measured virtual height are represented by their standard deviations. From a statistical point of view the 95% confidence limits of the mean virtual heights are about one fourth the standard deviations. However, considering all possible sources of error, the actual limits of uncertainty are probably about ± 1.5 km.

PRECEDING PAGE BLANK NOT FILMED

APPENDIX A-7

Calculated $N_e(z, \chi)$ Profiles

From a knowledge of how the Q-function changes with solar zenith angle (Appendix A-5) together with the noontime initial condition on the electron density profile (i.e. $N_e(\text{ref})$, Appendix A-6) we can calculate the decay of the electron density profile as the solar zenith angle proceeds toward sunset. This we do by considering the following photochemical equation for the rate of change of positive ion density.

$$dN_+/dt = Q - \alpha_d N_+ N_e - \alpha_i N_+ N_- \quad (1)$$

where α_d , α_i are the coefficients of electron-ion and ion-ion recombination respectively. Since

$$N_+ = N_e + N_- = (1 + \lambda) N_e \quad (2)$$

$$dN_+/dt = (1 + \lambda) dN_e/dt + N_e d\lambda/dt \quad (3)$$

Defining $\alpha_{eff} \equiv (1 + \lambda) (\alpha_d + \lambda \alpha_i)$, we then have

$$(1 + \lambda) dN_e/dt + N_e d\lambda/dt = Q - \alpha_{eff} N_e^2 \quad (4)$$

If we now assume that $\lambda \equiv N_-/N_e$ is time (zenith angle) independent, we have $d\lambda/dt = 0$ and equation (4) becomes

$$(1 + \lambda) dN_e/dt = Q - \alpha_{eff} N_e^2 \quad (5)$$

where α_{eff} is now time independent. This quantity can be evaluated by noting that at noontime (i.e. $\chi = 10^\circ$) $dN_e/dt = 0$, and therefore

$$\alpha_{eff} = Q(10^\circ)/N_e^2(\text{ref}) \quad (6)$$

For the special case $\lambda \ll 1$, equation (5) becomes

$$dN_e/dt = Q - \alpha_{eff} N_e^2 \quad (7)$$

which can be solved numerically. When this is done we find that the dN_e/dt term is completely negligible for $\chi \leq 75^\circ$. The decay of $N_e(z)$ with solar zenith angle can then be expressed as

$$N_e(z, \chi) = N_e(\text{ref}) \sqrt{\frac{Q(z, \chi)}{Q(z, 10^\circ)}} \quad (8)$$

The condition $\lambda \ll 1$ breaks down at some altitude $z \lesssim 80$ km. However since we have already determined that the dN_e/dt term is negligible for $\lambda \ll 1$, it immediately follows from equation (5) that dN_e/dt is even smaller when $\lambda \geq 1$. Thus within our assumption $d\lambda/dt = 0$, equation (8) remains a good approximation at the lower altitudes.

Profiles of $N_e(z, \chi)$ calculated from equation (8) are shown in Fig. A-7.1,2,3. The upper and lower limits on $N_e(z, \chi)$ shown in these figures result from the r.m.s. error $\Delta Q/Q$ given in Appendix A-5. Included in each figure is the $N_e(z)$ profile required above 95 km to yield agreement with the ground-based measurements of radiowave absorption and virtual height. It is seen that the required profiles are well outside the error limits on our calculated profiles.

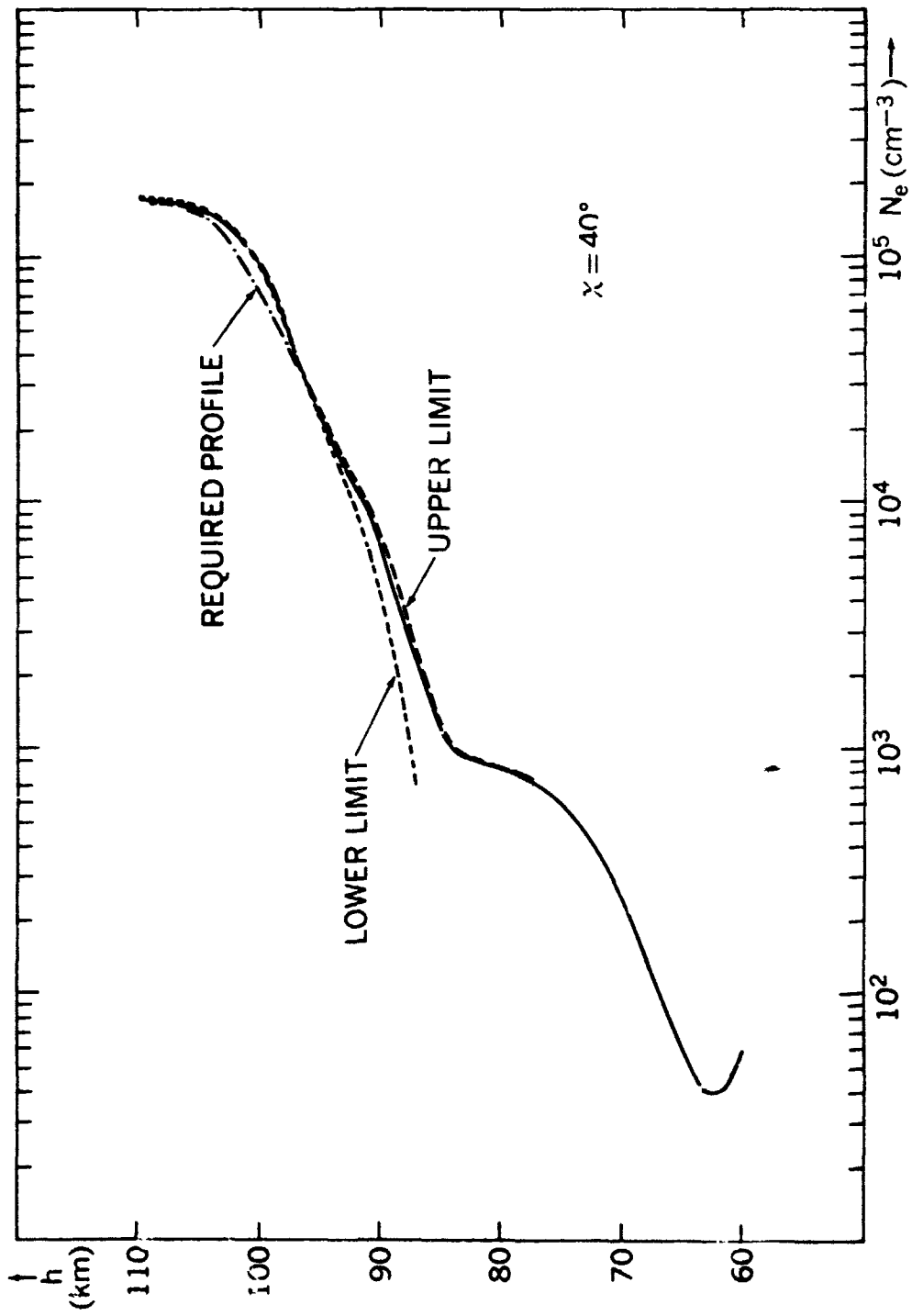


Figure A-7.1. At $\chi = 40^\circ$, required electron density profile compared with error limits on our calculated profile.

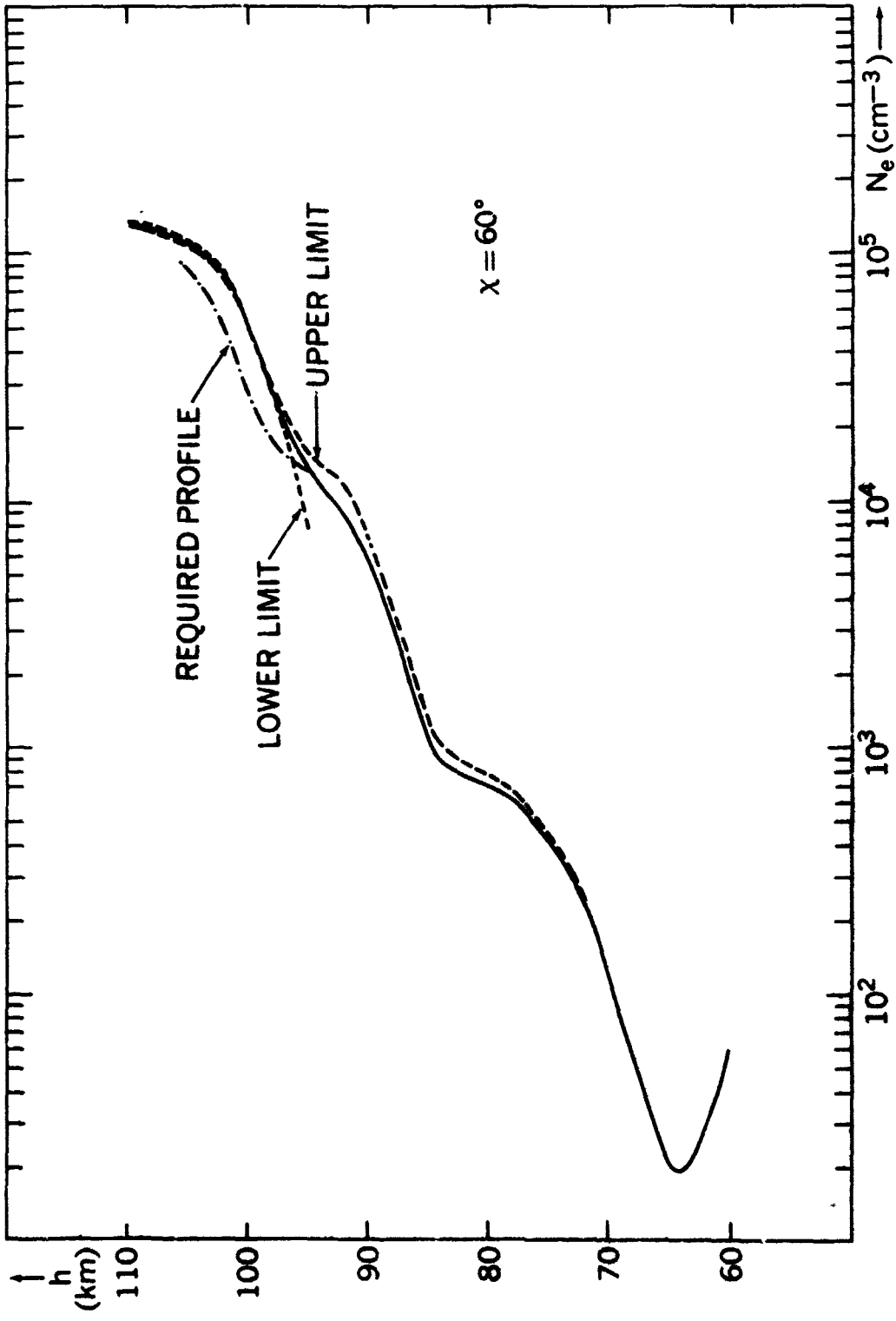


Figure A-7.2. At $\chi = 60^\circ$, required electron density profile compared with error limits on our calculated profile.

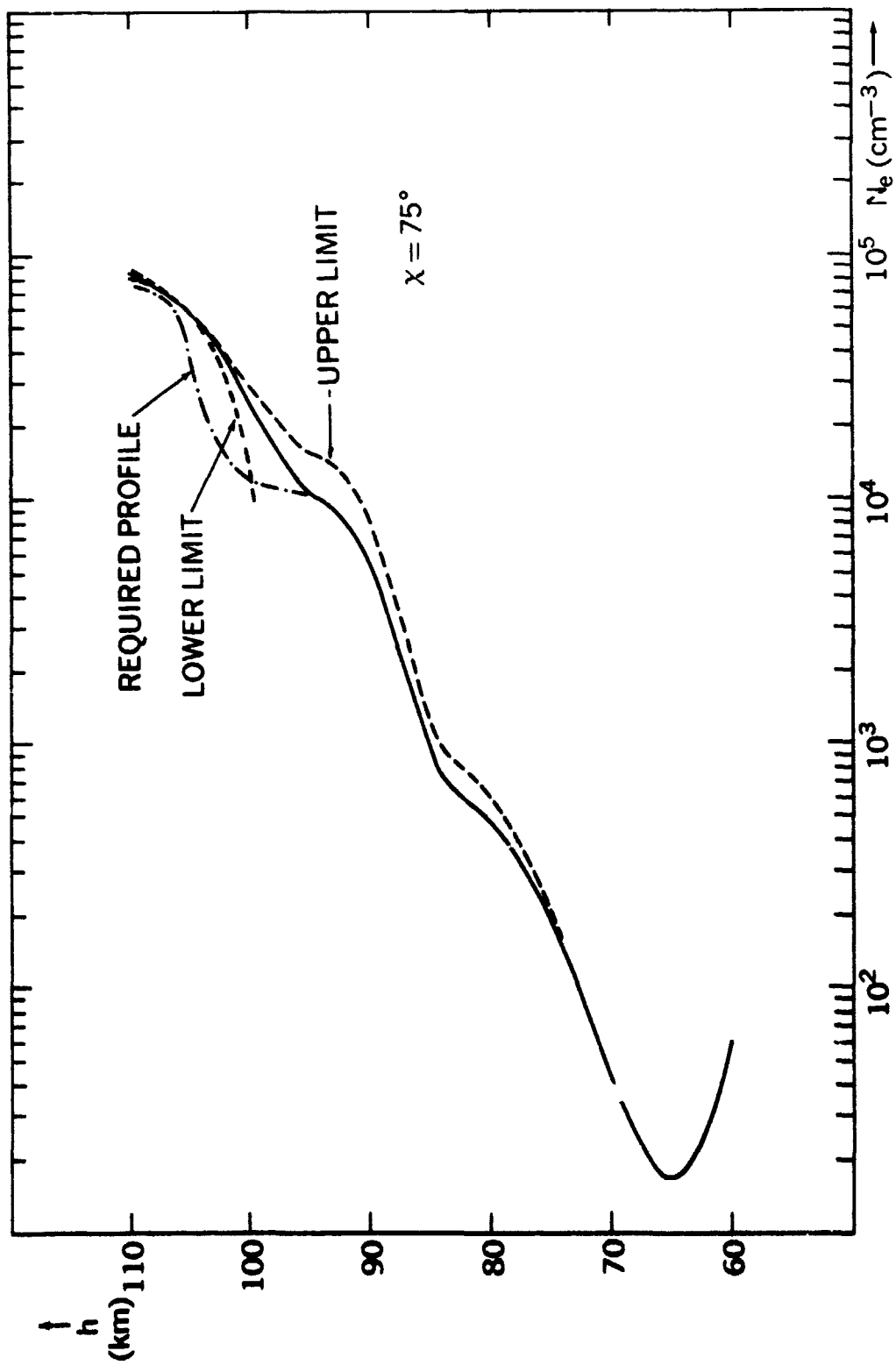


Figure A-7.3. At $\chi = 75^\circ$, required electron density profile compared with error limits on our calculated profile.

APPENDIX A-8

Equatorial $N_e(z, \chi)$ Model

Tabulated values of our model for the afternoon decay of the electron density profile (shown in Fig. 8, Section 10) are given here in Table A-8. It should be noted that this equatorial model is for equinoctial months under quiet sun conditions at solar cycle maximum. It should also be noted that at the lower-most altitudes our model underestimates the decay of the electron density profile since we have assumed that the effective recombination coefficient does not increase with solar zenith angle (i.e. $d\alpha/dt = 0$).

PRECEDING PAGE BLANK NOT FILMED

TABLE A-8

Alt (km)	$N_e(10^\circ)$ (cm^{-3})	$N_e(40^\circ)$ (cm^{-3})	$N_e(60^\circ)$ (cm^{-3})	$N_e(75^\circ)$ (cm^{-3})
6.10E1	7.50E1	4.58E1	4.26E1	4.26E1
6.20E1	8.50E1	4.00E1	3.08E1	3.08E1
6.30E1	9.50E1	4.12E1	2.24E1	2.24E1
6.40E1	1.10E2	4.98E1	1.92E1	1.82E1
6.50E1	1.30E2	6.41E1	2.01E1	1.70E1
6.60E1	1.55E2	8.37E1	2.54E1	1.79E1
6.70E1	1.90E2	1.11E2	3.63E1	2.07E1
6.80E1	2.30E2	1.45E2	5.32E1	2.50E1
6.90E1	2.90E2	1.96E2	8.09E1	3.26E1
7.00E1	3.50E2	2.50E2	1.16E2	4.18E1
7.10E1	4.20E2	3.15E2	1.63E2	5.53E1
7.20E1	5.00E2	3.92E2	2.23E2	7.58E1
7.30E1	5.70E2	4.63E2	2.85E2	1.03E2
7.40E1	6.30E2	5.27E2	3.49E2	1.38E2
7.50E1	6.80E2	5.84E2	4.10E2	1.80E2
7.60E1	7.40E2	6.49E2	4.80E2	2.33E2
7.70E1	7.80E2	6.97E2	5.38E2	2.88E2
7.80E1	8.40E2	7.61E2	6.10E2	3.55E2
7.90E1	9.80E2	8.07E2	6.66E2	4.19E2
8.00E1	9.10E2	8.42E2	7.13E2	4.78E2
8.10E1	9.30E2	8.67E2	7.49E2	5.31E2
8.20E1	9.50E2	8.89E2	7.81E2	5.80E2
8.30E1	9.85E2	9.23E2	8.22E2	6.36E2
8.40E1	1.07E3	1.00E3	9.00E2	7.21E2
8.50E1	1.30E3	1.21E3	1.10E3	9.06E2
8.60E1	1.85E3	1.70E3	1.55E3	1.31E3
8.70E1	2.75E3	2.48E3	2.25E3	1.95E3
8.80E1	4.00E3	3.48E3	3.14E3	2.27E3
8.90E1	5.80E3	4.86E3	4.32E3	3.88E3
9.00E1	8.20E3	6.61E3	5.71E3	5.18E3
9.10E1	1.12E4	8.62E3	7.11E3	6.47E3
9.20E1	1.55E4	1.13E4	8.78E3	7.93E3
9.30E1	2.10E4	1.44E4	1.04E4	9.17E3
9.40E1	2.70E4	1.76E4	1.15E4	9.78E3
9.50E1	3.55E4	2.25E4	1.30E4	1.06E4
9.60E1	4.75E4	2.60E4	1.42E4	1.08E4
9.70E1	6.20E4	3.10E4	1.55E4	1.10E4
9.80E1	8.00E4	3.90E4	1.80E4	1.12E4
9.90E1	1.00E5	5.00E4	2.15E4	1.15E4
1.00E2	1.22E5	6.60E4	2.70E4	1.21E4
1.01E2	1.44E5	8.60E4	3.80E4	1.32E4
1.02E2	1.62E5	1.07E5	5.00E4	1.50E4
1.03E2	1.76E5	1.25E5	6.20E4	1.80E4
1.04E2	1.85E5	1.40E5	7.20E4	2.50E4
1.05E2	1.90E5	1.51E5	8.50E4	3.90E4
1.06E2	1.90E5	1.50E5	9.70E4	5.60E4
1.07E2	1.90E5	1.65E5	1.08E5	6.50E4
1.08E2	1.90E5	1.65E5	1.15E5	7.10E4
1.09E2	1.90E5	1.65E5	1.20E5	7.30E4

ACKNOWLEDGEMENT

Part of this work was performed while one of us (S.G.) held a National Research Council Postdoctoral Resident Research Associateship.

REFERENCES

- Aikin, A. C., "Ionization Sources of the Ionospheric D and E Regions," Proceedings of the COSPAR Symposium on D- and E- Region Ion Chemistry (ed. by C. F. Sechrist, Jr., and M. A. Geller), p. 96, Univ. of Illinois, Urbana, Illinois, 1972.
- Aikin, A. C., and L. J. Blumle, "Rocket Measurements of the E-Region Electron Concentration Distribution in the Vicinity of the Geomagnetic Equator," J. Geophys. Res., 73, 1617, 1968.
- Aikin, A. C., R. A. Goldberg, Y. V. Somayajulu, and M. B. Avadhani, "Electron and Positive Ion Density Altitude Distributions in the Equatorial D-Region," J. Atmos. Terr. Phys., 34, 1483, 1972.
- Aikin, A. C., J. A. Kane, and J. Troim, "Some Results of Rocket Experiments in the Quiet D Region," J. Geophys. Res., 69, 4621, 1964.
- Argo, H. V., J. A. Bergey, and W. D. Evans, "Measurements of the Solar X-ray Flux in Selected Emission Lines," Astrophys. J., 160, 283, 1970.
- Austin, W. E., J. D. Purcell, R. Tousey, and K. G. Widing, "Coronal Emission-Line Intensities in the Extreme Ultraviolet," Astrophys. J., 145, 373, 1966.
- Banks, P., "Collision Frequencies and Energy Transfer," Planet. Space Sci., 14, 1085, 1966.
- Beynon, W. J. G., and S. Rangaswamy, "Model Electron Density Profiles for the Lower Ionosphere," J. Atmos. Terr. Phys., 31, 891, 1969.
- Blondi, M.A., "Atmospheric Electron-Ion and Ion-Ion Recombination Processes", Can. J. Chem., 47, 1711, 1969
- Blondi, M. A., M. T. Leu, and R. Johnsen, "Recombination of Electrons with Positive Ions of the $H_3O^+(H_2O)_n$ Series", Proceedings of the COSPAR Symposium on D- and E-Region Ion Chemistry (ed. by C. F. Sechrist, Jr., and M. A. Geller) p. 266, University of Illinois, Urbana, Illinois, 1972.
- Bruner, E. C., and R. W. Parker, "Hydrogen Geocorona and Solar Lyman-Alpha Line," J. Geophys. Res., 74, 107, 1969.
- Budden, K. G., "Radio Waves in the Ionosphere," Chapt. 10 Cambridge University Press, 1961.

- Byram, E. T., T. A. Chubb, H. Friedman, and J. E. Kupperian, "Observations of the Intensity of Solar Lyman-Alpha Emission," Astrophys. J., 124, 480, 1956.
- Byram, E. T., T. A. Chubb, H. Friedman, J. E. Kupperian, and R. W. Kreplin, "Intensity of Solar Lyman-Alpha and Adjacent Ultraviolet Emission Lines," Astrophys. J., 128, 738, 1958.
- Carver, J. H., P. Mitchell, E. L. Murray, and B. G. Hunt, "Molecular Oxygen Density and Lyman-Alpha Absorption in the Upper Atmosphere," J. Geophys. Res., 69, 3755, 1964.
- Chubb, T. A., H. Friedman, R. W. Kreplin, and J. E. Kupperian, "Lyman-Alpha and X-Ray Emissions During a Small Solar Flare," J. Geophys. Res., 62, 389, 1957.
- Detwiler, C. R., D. L. Garrett, J. D. Purcell, and R. Tousey, "The Intensity Distribution in the Ultraviolet Solar Spectrum," Ann. de Geophys., 17, 263, 1961.
- Eyfrig, R., and K. Rawer, quoted in "Synoptic Ionospheric Observations including Absorption, Drifts and Special Programmes" by K. Rawer, Chapt. 7, Annals of the IQSY Vol. 5, The M.I.T. Press, 1969.
- Freeman, F. F., and B. B. Jones, "Grazing Incidence Spectra of the Sun," Solar Physics, 15, 288, 1970.
- Gnanalingam, S., "An Apparatus for the Detection of Weak Ionospheric Echoes," Proc. I.E.E., 101, Pt. III, 243, 1954.
- Gnanalingam, S., "Equatorial Ionospheric Absorption during Half a Solar Cycle (1964-1970)" NASA-Goddard Space Flight Center Report X-625-72-276, July 1972 (to be published in J. Atmos. Terr. Phys.).
- Goldberg, R. A., "Positive Ion Composition Measurements in the D and E Regions of the Equatorial Ionosphere," Proceedings of the COSPAR Symposium on D- and E-Region Ion Chemistry (ed. by C.F. Sechrist, Jr., and M.A. Geller), p. 160, Univ. of Illinois, Urbana, Illinois, 1972.
- Goldberg, R. A., and A. C. Aikin, "Studies of Positive-Ion Composition in the Equatorial D-Region Ionosphere," J. Geophys. Res., 76, 8352, 1971.
- Groves, G. V., "Atmospheric Structure and its Variations in the Region From 25 to 120 km," Air Force Cambridge Research Laboratories: Environmental Research Paper No. 368, AFCRL-71-0410, 27th July, 1971.

- Hall, L. A., J. E. Higgins, C. W. Chagnon, and H. E. Hinteregger, "Solar-Cycle Variation of Extreme Ultraviolet Radiation," J. Geophys. Res., 74, 4181, 1969.
- Hall, L. A., and H. E. Hinteregger, "Solar Radiation in the Extreme Ultraviolet and its Variation with Solar Rotation," J. Geophys. Res., 75, 6959, 1970.
- Hall, L. A. W. Schweizer, and H. E. Hinteregger, "Long-term Variation of Solar Extreme Ultraviolet Fluxes," J. Geophys. Res., 70, 2241, 1965.
- Henke, B. L., and R. L. Elgin, "X-Ray Absorption Tables for the 2- to 200 Å Region," Advances in X-Ray Analysis Vol. 13 (ed. by B. L. Henke, J. B. Newkirk and G. R. Mallett), p. 633, Plenum Press, New York, 1970.
- Hinteregger, H. E., "The Extreme Ultraviolet Solar Spectrum and its Variation during a Solar Cycle," Ann. de Geophys., 26, 54., 1970.
- Hinteregger, H. E., L. A. Hall and G. Schmidtke, "Solar XUV Radiation and Neutral Particle Distribution in July 1963 Thermosphere," Space Research Vol. V, p. 1175, North-Holland, Amsterdam, 1965.
- Horan, D. M., "Coronal Electron Temperatures Associated with Solar Flares," Ph.D. Dissertation submitted to the Catholic University of America, Washington, D.C., Publication No. 70-22133, University Microfilms, Inc., 1970.
- Huffman, R. E., D. E. Pzulsen, J. C. Larrabee, and R. B. Cairns, "Decrease in D-Region O₂ (¹Δg) Photoionization Rates resulting from CO₂ Absorption," J. Geophys. Res., 76, 1028, 1971.
- Ivanov-Kholodnyi, G. S. and G. M. Nikol'skii, "The Sun and the Ionosphere," Chapt. VI, Izdatel'stvo "Nauka," Moscow, 1969 (English Translation available from U.S. Dept. of Commerce, Nat. Tech. Inf. Service, Springfield, Va. 22151).
- Jacchia, L. G., "Revised Static Models of the Thermosphere and Exosphere with Empirical Temperature Profiles," Smithsonian Astrophysical Observatory Special Report No. 332, Smithsonian Institution, Cambridge, Massachusetts 02138, 1971.
- Kane, J. A., "D Region Radio Measurements at the Magnetic Equator," NASA-Goddard Space Flight Center Report X-615-69-499, November 1969.
- Kane, J. A., "Evidence for the Existence of Negative Ions in the D- and Lower E-Regions at Twilight," NASA-Goddard Space Flight Center Report X-625-72-18, February 1972.

- Keneshea, T. J., "A Technique for Solving the General Reaction-Rate Equations in the Atmosphere," Air Force Cambridge Research Laboratories: Environmental Research Paper No. 263, AFCLR-67-0221, April 1967.
- Kreplin, R. W., "Solar X-Rays," Ann. de Geophys., 17, 153, 1961.
- Kreplin, R. W., and B. N. Gregory, "Solar X-Ray Monitoring During the IQSY," Space Research VI, p. 1011, North-Holland Publishing Co., Amsterdam, 1966.
- Kreplin, R. W., and D. M. Horan, "The NRL Solrad 9 Satellite - Solar Explorer B-1938-17A," NRL Report 6800, p. 39, March 1969.
- Lyon, A. J., "Solar Cycle and Annual Variations of the E Layer Electron Density at Ibadan," Proceedings of the Second International Symposium on Equatorial Aeronomy (ed. by F. de Mendonca), p. 88, National Commission for Space Activities, Sao Paulo, Brazil, 1965.
- Manson, J. E., "The Spectrum of the Quiet Sun Between 30 and 128 Å for November 1965," Astrophys. J., 147, 703, 1967.
- Manson, J. E., "Instrumental Recalibration and Refinement of Solar Ultrasoft X-Ray Intensities," Astrophys. J., 153 (letters) p. 191, 1968.
- Manson, J. E., "Measurements of the Solar Spectrum between 30 and 128 Å," Solar Physics 27, p. 107, Nov. 1972.
- Meier, R. R., and P. Mange, "Geocoronal Hydrogen: An Analysis of the Lyman-Alpha Airglow Observed from OGO-4," Planet, Space Sci., 19, 803, 1970.
- Meira, L. G., Jr., "Rocket Measurements of Upper Atmospheric Nitric Oxide and their Consequences to the Lower Ionosphere," J. Geophys. Res., 76, 202, 1971.
- Minnis, C. M., "Ionospheric Indices." In Advances in Radio Research (ed. by J. A. Saxton), Academic Press, London, 1964.
- Mitra, A. P., Private Communication, 1968.
- Neupert, W. M., "X-Rays from the Sun," Ann. Rev. Astron. Ap., 7, 121, 1969.
- Ohshio, M., R. Maeda, and H. Sakagami, "Height Distribution of Local Photoionization Efficiency," J. Radio Res. Labs., 13, 245, 1966.

- Paulsen, D. E., R. E. Huffman, and J. C. Larrabee, "Improved Photoionization Rates of O_2 ($^1\Delta_g$) in the D Region," Radio Sci., 7, 51, 1972.
- Phelps, A. V., "Electron Collision Frequencies and Radio Frequency Absorption," Chapt. 21, DASA Reaction Rate Handbook, 1972.
- Piggott, W. R., and E. V. Thrane, "The Electron Densities in the E- and D-Regions above Kjeller," J. Atmos. Terr. Phys., 28, 467, 1966.
- Pounds, K. A., "The Solar X-Radiation below 25 \AA ," Ann. de Geophys., 26, 555, 1970.
- Satya Prakash, B. H. Subbaraya, and S. F. Gupta, "Investigation of the Daytime Lower Ionosphere over the Equator Using Langmuir Probe and Plasma Noise Probe," J. Atmos. Terr. Phys., 33, 129, 1972.
- Somayajulu, Y. V., M. B. Avadhanulu, K. S. Zalpuri, and S. C. Garg, "Some Preliminary Results of Rocket Sounding of the D Region at the Geomagnetic Equator," Space Research XI, p. 1131, Akademie-Verlag, Berlin 1971.
- Swider, W., Jr., "Ionization Rates due to the Attenuation of 1-100 \AA Nonflare Solar X-Rays in the Terrestrial Atmosphere," Rev. Geophys., 7, 573, 1969.
- Thorpe, M. R., "The Phase Integral Correction for Calculations of Radio Wave Absorption in the Ionosphere," J. Atmos. Terr. Phys., 33, 1597, 1971.
- Witheridge, J. E., "Calculation of the Virtual Height and Absorption of Radio Waves in the Ionosphere," Radio Sci., 2, 133, 1967.
- Tousey, R., "The Lyman Alpha Line in Space," XIII Internat. Astr. Congress, Varna 1962 (ed. by N. Boneff and I. Hersey), p. 156, Springer-Verlag, Vienna, 1964.
- Van Allen, J. A., "The Nature and Intensity of the Cosmic Radiation," in Physics and Medicine of the Upper Atmosphere (ed. by C. S. White and O. O. Benson, Jr.) University of New Mexico Press, Albuquerque, 1952.
- Weeks, L. H., "Lyman-Alpha Emission from the Sun near Solar Minimum," Astrophys. J. (letters), 147, 1203, 1967.
- Yefremov, A. I., A. L. Podmoshensky, O. N. Yefimov, and A. A. Lebedev, "Investigations of Solar X-Rays and Lyman-Alpha Radiation on August 19-20, 1960," Space Research III, p. 843, North-Holland, Amsterdam, 1963.